

# Understanding cell populations sharing information through the environment, as reinforcement learning

Masaki Kato, Tetsuya J. Kobayashi

*Department of Mathematical Informatics,  
the Graduate school of Information Science and Technology,  
the University of Tokyo, Tokyo, Japan*

(Dated: July 23, 2024)

arXiv:2407.15298v1 [q-bio.CB] 21 Jul 2024

# Abstract

Collective migration is a phenomenon observed in various biological systems, where the cooperation of multiple cells leads to complex functions beyond individual capabilities, such as in immunity and development. A distinctive example is cell populations that not only ascend attractant gradient originating from targets, such as damaged tissue, but also actively modify the gradient, through their own production and degradation. While the optimality of single-cell information processing has been extensively studied, the optimality of the collective information processing that includes gradient sensing and gradient generation, remains underexplored. In this study, we formulated a cell population that produces and degrades an attractant while exploring the environment as an agent population performing distributed reinforcement learning. We demonstrated the existence of optimal couplings between gradient sensing and gradient generation, showing that the optimal gradient generation qualitatively differs depending on whether the gradient sensing is logarithmic or linear. The derived dynamics have a structure homogeneous to the Keller-Segel model, suggesting that cell populations might be learning. Additionally, we showed that the distributed information processing structure of the agent population enables a proportion of the population to robustly accumulate at the target. Our results provide a quantitative foundation for understanding the collective information processing mediated by attractants in extracellular environments.

## CONTENTS

|                                                                                                  |    |
|--------------------------------------------------------------------------------------------------|----|
| I. Introduction                                                                                  | 3  |
| II. Model                                                                                        | 5  |
| A. Reinforcement learning formulation of the exploration problem                                 | 5  |
| B. A distributed learning model for an agent population                                          | 9  |
| III. Model property: Comparison of the continuous limit to existing collective chemotaxis models | 12 |
| IV. Numerical experiments                                                                        | 15 |
| A. Demonstration through maze-solving                                                            | 15 |
| B. Optimality evaluation                                                                         | 19 |

|                                                                |     |
|----------------------------------------------------------------|-----|
| C. Comparison with a single-agent system                       | 22  |
| V. Discussion                                                  | 25  |
| A. Conclusion                                                  | 25  |
| B. Discussion                                                  | 25  |
| Acknowledgments                                                | 28  |
| References                                                     | 28  |
| A. A brief review of reinforcement learning                    | S1  |
| 1. Conventional MDP and RL                                     | S1  |
| 2. Entropy-regularized MDP and RL                              | S3  |
| B. Derivation of the update equations and continuous limits    | S7  |
| 1. Derivation of the intrinsic cue concentraion updates        | S7  |
| 2. Derivation of the continuous limits                         | S7  |
| a. Continuous limit of agents' motility                        | S8  |
| b. Continuous limit of the intrinsic cue concentration updates | S10 |
| C. Supplemental experiments                                    | S11 |
| 1. Maze solving with other couplings                           | S11 |
| 2. Supplemental figures for Section IV B                       | S14 |

## I. INTRODUCTION

Collective migration is a widespread phenomenon observed across biological systems, from immunity to morphogenesis [1]. Cooperation of multiple cells in migration leads to complex functions beyond individual capabilities, such as in immunity [2] and development [3]. A distinctive example is cell populations that indirectly share positional information of target, such as damaged tissue, by actively modifying attractant gradients through their own production and degradation (Figure 1). Cells not only climb attractant gradients but also degrade the attractants to create their own gradients, enabling efficient migration into unexplored areas [4]. Additionally, cells that have reached the target produce the attractants to recruit other cells and enhance accumulation [5]. Such production and degradation

mechanisms enable cell populations like *Dictyostelium discoideum* to cooperatively alter attractants gradients, solving complex mazes [6]. This indirect information sharing through the environment is observed in various cell populations, including immune [7, 8] and cancer cells [9], and is believed to enable such small cells with simple sensing capability to efficiently share information across vast environments and achieve advanced migration [4].

Despite accumulating insights into collective migration mediated by attractant production and degradation in molecular and cell biology, there has been little theoretical investigation into their function and optimality, such as their efficiency. Recent studies on the function of responses to environmental attractants have focused on single-cell chemotaxis, particularly bacterial gradient responses. It has been experimentally and theoretically revealed that bacteria respond linearly in low attractant concentration and logarithmically in high concentration [10, 11], along with underlying biophysical principles [12]. Furthermore, based on biophysical models, the optimality of bacterial gradient responses has been discussed [13–15]. Expanding the study of chemotaxis functionality from single-cell chemotaxis to collective chemotaxis remains a future challenge. Already, the unique properties of collective chemotaxis are being experimentally and theoretically elucidated, including cell population motility [16, 17], individual traits’ impact on population behavior [18, 19], intercellular communication in collective sensing [20–23], the interplay with growth [24] and evolution [25].

However, the optimality of collective chemotaxis is less investigated compared to single-cell chemotaxis, leaving unresolved issues that cannot be addressed by single-cell insights alone. One issue is the consistency and optimality of attractant degradation and production for optimal migration in collective chemotaxis by eukaryotic cell populations. In cases of neutrophils, which generate their own concentration fields by producing and degrading attractants, focusing only on gradient responses to external attractants, as in single bacterial cells, is insufficient for addressing optimal migration. Optimal migration requires the self-generated concentration field consistent with the gradient sensing for fast and prolonged accumulation. A recent study have theoretically discussed the optimality of collective search induced by attractants using optimal control theory [26]. The study addresses optimal gradient sensing to optimally-generated attractant field but heuristically incorporates the generation process of the field, lacking consistency and optimality in the coupling between gradient sensing and field generation.

Another issue is comparing collective information processing with single-agent information processing. Collective information processing enables agents with limited capabilities, such as cells with restricted memory capacity, to accomplish specific tasks as a group, while a single agent with sufficient capabilities, such as higher organisms, can also perform the same tasks. However, the advantages and disadvantages of collective information processing compared to a single-agent information processing are unclear. The issues of processing structure in functionality are biologically significant because they relate to understanding why individually advanced organisms have evolved, and why collective information processing has been evolutionarily maintained.

This study formulates a cell population exploring the environment through attractant production and degradation as agents performing distributed reinforcement learning, clarifying the optimal coupling between attractant field generation and sensing, and the functionality of distributed structure. Specifically, by associating the state value in reinforcement learning (i.e., the likelihood of accumulating at the target) with attractant concentration in the environment, we show that the process by which individual cells cooperatively modifying attractant concentration based on their local observation can be interpreted as agents learning the optimal state value in a distributed manner based on their experiences. (Figure 2). The derived dynamics are homologous to the Keller-Segel model, widely used to explain experimental results of collective chemotaxis, suggesting that cell populations may perform distributed learning. Furthermore, we derive two qualitatively different equations for optimal attractant production and degradation, depending on whether the sensing to concentration gradients is linear or logarithmic. Finally, comparing with a single smart agent with complete internal memory, we demonstrate that the unsmart agent population, which distributedly learns via external attractant, can robustly achieve the portion of the population at the target.

## II. MODEL

### A. Reinforcement learning formulation of the exploration problem

We represent the environment as an undirected graph  $G = (\mathcal{S}, \mathcal{E})$  with a finite set of vertices  $\mathcal{S}$  and a finite set of edges  $\mathcal{E}$  to address the general spatial topology explored by an

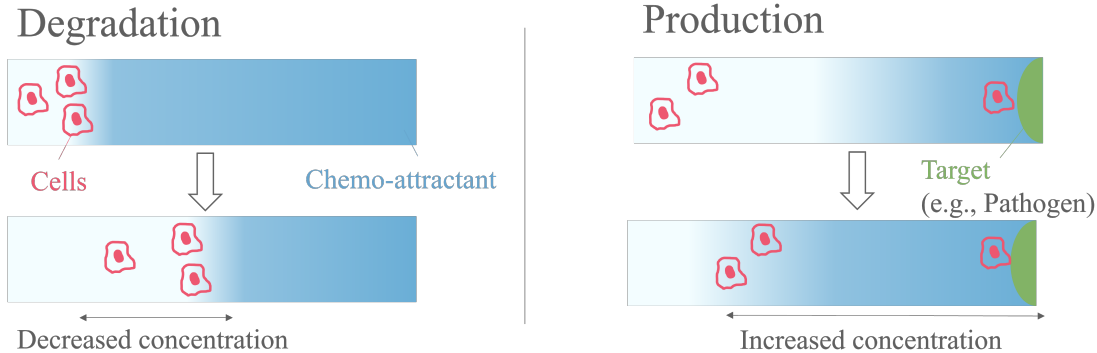


FIG. 1. Schematics of attractant degradation and production by a cell population.

agent population. In the environment,  $N \in \mathbb{Z}_+$  homogeneous and independent agents locate at the vertices of the graph with overlap, transitioning between vertices without direct interaction in discrete time: at time  $t \in \{0, 1, \dots\}$ , agent  $i \in \{1, 2, \dots, N\}$  has the state  $s_t^i \in \mathcal{S}$ . At time  $t$ , when agent  $i$  transitions from vertex  $s$ , the next vertex is stochastically chosen according to the transition probability  $\pi_t^i(\cdot|s) \in \Delta(\mathcal{S})$ , referred to as the agent's behavior policy. The larger  $\pi_t^i(s'|s)$ , the more likely agent  $i$  at vertex  $s$  is to move to vertex  $s'$  at the next time step. Assuming small unit time, transitions are restricted to the current vertex and its neighbors:  $\pi_t^i(s'|s) > 0$  if  $s' \in \{s\} \cup \mathcal{N}(s)$ ,  $\pi_t^i(s'|s) = 0$  otherwise. Here,  $\mathcal{N}(s)$  denotes the set of neighboring vertices of vertex  $s$ :  $\mathcal{N}(s) := \{s' \in \mathcal{S} | e_{ss'} \in \mathcal{E}\}$ .

Each agent is assumed to learn a better policy  $\pi_t^i$  moving to a vertex closer to the target through exploration, rather than continuously following the same policy. For single-celled organisms without a complete internal memory, learning a better policy is achieved through multiple molecule signals in the environment [27]. One of these signaling molecules is a (primary) extrinsic guidance cue, not controlled by the agents. The extrinsic cue concentration convey local information about the targets' position, assumed to be represented by a reward function  $r : \mathcal{S} \rightarrow \mathbb{R}_{\geq 0}$ . For example,  $r(s) = 1$  if  $s = s^0$  and  $r(s) = 0$  otherwise describes a target exists only at vertex  $s^0 \in \mathcal{S}$ . More realistically, the decreasing function  $r(s) = \exp(-l(s; s^0))$  with distance  $l(s; s^0)$  from the target (damaged tissue) represents fMLP concentration originating from damaged tissue [28]. Generally, extrinsic cues may change over time due to agents and the environment, but, for simplicity, this study assumes that they depend only on the targets' position and magnitude and are not altered by the agents. Examples of target magnitude variations include tissue damage size or the number

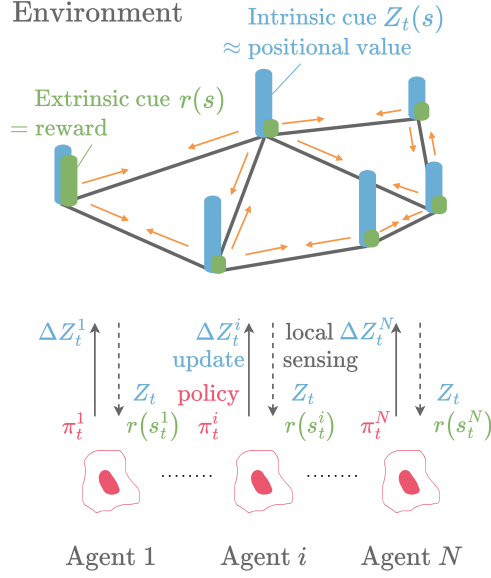


FIG. 2. A schematic diagram of an agent population learning optimal migration in a distributed manner via the environment. The optimal state value  $V^*$  for optimal migration is determined by the time-invariant concentration  $r$  of extrinsic cue, which contain the positional information of the targets in the environment. Agents learn  $V^*$  by associating intrinsic cue concentration  $Z_t$  with their estimation of  $V^*$  ( $V^* \approx \mathcal{F}[Z_t]$ ). Each agent  $i \in \{1, \dots, N\}$  senses surrounding  $Z_t$  and local  $r$  at each time step. Based on the sensed  $r$  and  $Z_t$ , each agent moves with its policy  $\pi_t^i$  and outputs individual update  $\Delta Z_t^i = \Delta Z_t(s_t^i)$  to the environment.

of localized necrotic cells in neutrophil accumulation. In fact, neutrophils do not accumulate at small necrotic lesions where resident immune cells respond immediately [29]. However, due to factors such as harsh environments and their instability, extrinsic cues decay rapidly and are less likely to transmit over long distances. To amplify the decaying extrinsic cue, cell populations utilize (secondary) intrinsic cues,  $Z_t : \mathcal{S} \rightarrow \mathbb{R}_{\geq 0}$ , controlled by individual cells. For example, neutrophils sense extrinsic cues such as fMLP and C5a from damaged tissue, and they actively produce and release more diffusible intrinsic cues, such as LTB4, packaged in vesicles or exosomes to convey information to distant immune cells [30–32]. In this study, we assume that agents receive the target information from the signaling cue concentrations  $(Z_t(s), r(s))$  in their vicinity, and based on the information, update the intrinsic cue concentration  $Z_t$  to improve the policy  $\pi_t^i$  for accumulating at the target in a distributed manner. For simplicity, we assume that at time  $t$ , agent  $i$  at vertex  $s_t^i$  can sense  $(Z_t(s))_{s \in \{s_t^i\} \cup \mathcal{N}(s_t^i)}$

and  $r(s_t^i)$  with sufficient accuracy.

In this study, we consider the process by which agents learn a policy to quickly reach and remain at the target represented by the extrinsic cue  $r$  by modifying the intrinsic cue  $Z_t$  shared within the environment. We associate the extrinsic cue concentration  $r$  with the reward function in reinforcement learning and formulate the problem as learning the optimal policy  $\pi^* = \operatorname{argmax}_{\pi} \mathcal{J}[\pi]$  that maximizes the following expected cumulative discounted regularized reward  $\mathcal{J}[\pi]$ :

$$\mathcal{J}[\pi] := E \left[ \sum_{t=0}^{\infty} \gamma^t R^{\pi}(s_t, s_{t+1}) \right], \quad (1)$$

$$R^{\pi}(s_t, s_{t+1}) = r(s_t) - \frac{1}{\beta} \log \frac{\pi(s_{t+1}|s_t)}{p(s_{t+1}|s_t)}, \quad (2)$$

where the expected value  $E[f(s_{0:t})]$  is the path average of  $f(s_{0:t})$  on the state sequences  $s_0, s_1, \dots, s_t$ , and discount factor  $\gamma \in [0, 1)$  is an intrinsic parameter common to all agents, indicating how past sensed extrinsic cues are weighted. It is reasonable for simple organisms with limited memory to emphasize the near future since the influence of current situation diminishes due to environmental noise and other factors. In Eq. (2), besides the locally-sensed extrinsic cue concentration  $r$ , there is a control penalty  $\frac{1}{\beta} \log \frac{\pi}{p}$  for the policy  $\pi$  that deviates from the intrinsic (stationary) transition probability  $p : \mathcal{S} \times \mathcal{S} \rightarrow [0, 1]$ . The intrinsic transition probability corresponds to the random motility exhibited spontaneously by cells, and the penalty corresponds to the motility control cost for deviating from this probability in a cue-dependent manner. Note that inverse control weight  $\beta \in (0, \infty)$  represents the ease of motility control and is assumed to be a common for all agents. The formulation in Eq. (1) is identical to the entropy-regularized Markov decision process [33] (Appendix. A 2). Defining the state value function  $V^{\pi} : \mathcal{S} \rightarrow \mathbb{R}$  and the optimal state value function  $V^* : \mathcal{S} \rightarrow \mathbb{R}$ :

$$V^{\pi}(s) := E \left[ \sum_{t=0}^{\infty} \gamma^t R^{\pi}(s_t, s_{t+1}) \middle| s_0 = s \right] \quad s \in \mathcal{S}, \quad (3)$$

$$V^*(s) := \max_{\pi} V^{\pi}(s) \quad s \in \mathcal{S}, \quad (4)$$

the optimal policy  $\pi^*$  can be explicitly written using the optimal state value  $V^*$  as follows:

$$\pi^*(s'|s) = \frac{p(s'|s) \exp(\beta \gamma V^*(s'))}{\sum_{s' \in \mathcal{S}} p(s'|s) \exp(\beta \gamma V^*(s'))} \quad s, s' \in \mathcal{S}. \quad (5)$$

The optimal policy  $\pi^*$  varies with the extrinsic cue  $r$  that defines the exploration environment. Each agent updates its current policy  $\pi_t^i$  by modifying the intrinsic cue concentration

$Z_t$  while receiving local information about  $r$  through exploration of the unknown environment, thereby learning the optimal policy  $\pi^*$ . Furthermore, we assume that the population approximates the optimal state value  $V^*(s)$  by a function of the intrinsic cue concentration  $Z_t(s)$  ( $V^*(s) \approx \mathcal{F}[Z_t](s)$ ) and learns  $V^*$  collectively through the production and degradation of intrinsic cue.

Pezzotta et al. [26] highlighted that a cell population ascending an optimized intrinsic cue gradient can be interpreted as an optimally controlled agent population ascending the optimal state value gradient employing stochastic optimal control theory. We extend this idea to reinforcement learning theory, considering an agent population where each agent ascends the intrinsic cue gradient while cooperatively adjusting the gradient based on the sensed extrinsic cue concentration. This approach addresses not only the optimal behaviors but also the learning process towards optimality, suggesting the optimal relationship between the generation of the intrinsic cue field and the sensing to that field.

## B. A distributed learning model for an agent population

Multiple mapping  $\mathcal{F}[Z]$  can relate the optimal state value to the intrinsic cue concentration. One mapping associate the logarithm of the intrinsic cue concentration with an estimate of the optimal state value:  $V^*(s) \approx \mathcal{F}[Z_t](s) := \log(Z_t(s))/\beta$ . Here, there exists an optimal intrinsic cue concentration  $Z^* : \mathcal{S} \rightarrow \mathbb{R}_{\geq 0}$  that is in bijective correspondence with  $V^*$  through  $\mathcal{F}$  ( $V^*(s) = \mathcal{F}[Z^*](s)$ ,  $s \in \mathcal{S}$ ).

After learning, if  $Z_t$  closely approximates  $V^*$  (equivalently,  $Z_t(s) = Z^*(s)$  for  $s \in \mathcal{S}$ ), then according to Eq. (5), an agent  $i$  at vertex  $s_t^i$  at time  $t$  will transition following the policy  $\pi_t$ , which depends on the surrounding  $Z_t$ :

$$s_{t+1}^i \sim \pi_t(\cdot | s_t^i) := \frac{p(\cdot | s_t^i) Z_t^\gamma(\cdot)}{\sum_{s' \in \mathcal{S}} p(s' | s_t^i) Z_t^\gamma(s')}, \quad \forall i \in \{1, 2, \dots, N\}. \quad (6)$$

In the following, we assume that during the learning process, the agents respond to current  $Z_t$  by following the same policy (6). This assumes that agents lack internal memory and move based solely on surrounding intrinsic cue concentration  $Z_t$ , indirectly interacting to others. Eq. (6) represents agents' chemotactic behavior that basically follows the intrinsic transition probability  $p$  but deviates towards higher  $Z_t$ . When  $Z_t(s)$  closely approximates  $V^*(s)$  (4) determined by extrinsic cue, agents move to vertices with higher state values, thus

approaching the target.

Therefore, the intrinsic cue production and degradation for learning  $V^*$  should update the current intrinsic cue concentration  $Z_t$  to approximate the optimal  $Z^*$ . We consider the simplest dynamics that approximately minimize the following cost function  $\mathcal{C}[Z_t]$ , which incorporates the squared error between the  $Z_t$  and  $Z^*$  and the physical constraint of diffusion associated with the intrinsic cue:

$$\mathcal{C}[Z_t] := \frac{N}{2} \sum_{s \in \mathcal{S}} \mu^{\pi_t}(s) (Z^*(s) - Z_t(s))^2 - \frac{D}{2\alpha} \sum_{s, s' \in \mathcal{S}} L_{ss'} Z_t(s) Z_t(s'), \quad (7)$$

where  $\mu^{\pi_t}(s)$  denotes the stationary distribution of  $\pi_t$ ,  $D \in \mathbb{R}_+$  represents the diffusion coefficient,  $\alpha \in (0, 1/N)$  represents the time scale of the intrinsic cue production and degradation by agents, and  $L$  denotes the graph Laplacian of the environment  $\mathcal{G}$ . The second term of Eq. (7) accounts for diffusion effects. The larger diffusion coefficient relative to the intrinsic cue production and degradation, the stronger the diffusion becomes, particularly at vertices with fewer agents.

We assume that an agent population sequentially and distributively updates the intrinsic cue concentration at each cell's position, thus collectively learning an optimal intrinsic cue concentration. This updating process does not require the memory of past positions or sensed concentrations, making it feasible for simple cells. The simplest sequential update is gradient descent on  $\mathcal{C}[Z_t]$ ; but it requires complete knowledge of the optimal concentration  $Z^*$ , which is not biologically plausible. In reinforcement learning theory, a method called semi-gradient descent [34, 35] has been proposed to approximate the gradient by using only the current estimate  $Z_t$  and the immediate reward  $r(s_t)$ . This study applies the idea of semi-gradient descent, employing an approximate gradient descent on  $\mathcal{C}[Z_t]$  using the locally sensed current intrinsic cue concentration  $Z_t$  and extrinsic cue concentration  $r$  by a finite homogeneous population of  $N$  agents (derivation is provided in Appendix. B1):

$$Z_{t+1}(s) - Z_t(s) = - \sum_{i=1}^N \mathbb{1}_{s_t^i=s} \alpha \Delta Z_t(s_t^i) \quad (8a)$$

$$-D \sum_{s' \in \mathcal{S}} L_{ss'} Z_t(s'), \quad s \in \mathcal{S} \quad (8b)$$

$$\Delta Z_t(s) := Z_t(s) - \exp(\beta r(s)) \sum_{s' \in \mathcal{S}} p(s'|s) Z_t(s'), \quad (8c)$$

where  $\mathbb{1}_{s_t^i=s}$  is an indicator function that takes 1 if agent  $i$  is at vertex  $s$  at time  $t$  and 0 otherwise. In Eq. (8), each agent at  $s_t^i$  outputs individual update  $\alpha \Delta Z_t(s_t^i)$  to the environment,

based on the estimated error (TD error) calculated from the locally sensed  $r$  and surrounding  $Z_t$ .  $Z_t$  is updated by the sum of the individual updates, while it diffuses to neighbors independently of the agents at a constant rate (Figure 2). This learning dynamics is a distributed version of Greedy Z-learning [33], a variant of TD-learning, with a sequential regularization.

Greedy Z-learning has three advantages from both biological and learning theory perspectives: First, it incorporates the agent’s motility control cost as KL divergence from the intrinsic motility (Eq. (2)). Second, due to policy regularization (Eq. (2)), both the optimal policy (5) and its update (8) avoids max operator, making it less susceptible to noise and more biologically natural. Third, it allows off-policy learning of the optimal policy (Eq. (5)) through a sequential process while following a stochastic policy (6) similar to the Boltzmann policy. Based on the mapping between the logarithm of the intrinsic cue concentration and the optimal state value  $V^*(s) \approx \mathcal{F}[Z_t](s) = \log(Z_t(s))/\beta$ , we refer to this learning model for the agent population (6), (8) as the log-exp coupling model, inspired by its continuous limit form (Eq. (13)).

Thus, we can formulate the environmental exploration problem by an agent population as an entropy-regularized Markov decision process without explicit actions [33]:  $(\mathcal{S}, r, p, \gamma, \beta)$ , comprising the state space  $\mathcal{S}$  of agents’ exploration environment  $\mathcal{G}$ , the extrinsic cue concentration  $r$  in the environment, the intrinsic transition probability  $p$  dependent on  $\mathcal{G}$ , and the parameters  $\gamma$  and  $\beta$  intrinsic to the agents. Furthermore, the exploration process by the agent population is formulated as a distributed reinforcement learning [36], where  $N$  agents learn the optimal migration policy through the shared intrinsic cue.

The previously introduced log-exp coupling model is based on the mapping between the logarithm of the intrinsic cue concentration and the estimated state value, consistent with the logarithmic gradient sensing observed in chemotaxis. However, sometimes the absolute concentration is sensed instead of the logarithm [10, 11]. The absolute gradient sensing can also be theoretically captured by considering another mapping  $\mathcal{F}$  between the intrinsic cue concentration  $Z_t(s)$  as the estimated state value:  $V^*(s) \approx \mathcal{F}[Z_t](s) = Z_t(s)/\beta$ . Based on this mapping, each agent’s policy is as follows:

$$s_{t+1}^i \sim \pi_t(\cdot | s_t^i) := \frac{p(\cdot | s_t^i) \exp(\gamma Z_t(\cdot))}{\sum_{s' \in \mathcal{S}} p(s' | s_t^i) \exp(\gamma Z_t(s'))}, \quad \forall i \in \{1, 2, \dots, N\}. \quad (9)$$

Unlike Eq. (6), the agents transition to vertices weighted by the exponent of  $Z_t$ . Similar to

Eq. (6), if  $Z_t$  closely approximate  $V^*$  ( $V^*(s) = \mathcal{F}[Z_t](s)$ ), then  $\pi_t$  is the optimal policy  $\pi^*$ , and the optimal intrinsic cue concentration  $Z^*$  exists in bijective correspondence with the  $V^*$  through  $\mathcal{F}$ . Similarly, we obtain the corresponding update of the intrinsic cue concentration:

$$Z_{t+1}(s) - Z_t(s) = - \sum_{i=1}^N \mathbb{1}_{s_t^i=s} \alpha \Delta Z_t(s_t^i) - D \sum_{s' \in \mathcal{S}} L_{ss'} Z_t(s'), \quad s \in \mathcal{S}, \quad (10a)$$

$$\Delta Z_t(s) := Z_t(s) - \beta r(s) - \ln \sum_{s' \in \mathcal{S}} p(s'|s) \exp(\gamma Z_t(s')). \quad (10b)$$

Also, we obtain the corresponding cost function  $\mathcal{C}[Z_t]$ :

$$\mathcal{C}[Z_t] := \frac{N}{2} \sum_{s \in \mathcal{S}} \mu^{\pi_t}(s) (Z^*(s) - Z_t(s))^2 - \frac{D}{2\alpha} \sum_{s, s' \in \mathcal{S}} L_{ss'} Z_t(s) Z_t(s'). \quad (11)$$

Similar to Eq. (8), at each time step,  $Z_t$  is updated by the sum of the individual updates  $\alpha \Delta Z_t(s_t^i)$  based on local sensing, with constant diffusion. Due to the different mapping  $\mathcal{F}$ , the individual update (10b) differs from Eq. (8c). This learning dynamics is a distributed and sequentially regularized version of (Greedy) G-learning [37], which has the same advantages as Z-learning. We refer to this model (9), (10) based on the linear mapping, as the lin-lin coupling model, inspired by its continuous limit form (14).

### III. MODEL PROPERTY: COMPARISON OF THE CONTINUOUS LIMIT TO EXISTING COLLECTIVE CHEMOTAXIS MODELS

Thus far, we have considered discrete space and time dynamics in relation to reinforcement learning, but to relate the dynamics to existing phenomena, we need its continuous limit dynamics. In this section, we confirm that the log-exp coupling model (6), (8) and the lin-lin coupling model (9), (10), each a discrete space-time stochastic model, have a structure homologous to the well-known Keller-Segel equations [38, 39], representative partial differential equations for collective chemotaxis, in appropriate continuous space-time limits (TABLE I).

For simplicity, we consider a one-dimensional lattice  $\mathcal{S} = S^h := \{0, \pm h, \pm 2h, \dots\}$  with a uniform spacing  $h$  and define the agents' intrinsic transition probability  $p^h : S^h \times S^h \rightarrow [0, 1]$  as a lazy random walk, such that  $p^h(x|x) = \varepsilon^h(x) = O(h)$ ,  $p^h(x \pm h|x) = (1 - \varepsilon^h(x))/2$ . Under an appropriate time scale and in the limit of infinite agents, the continuous space-time

limits  $h \rightarrow 0$  of the log-exp and lin-lin coupling models correspond to the following pairs of one-dimensional partial differential equations (derivation is provided in Appendix B 2):

$$\partial_t \mu(t, x) = -\nabla \cdot (\mu(t, x) \psi(\nabla Z(t, x), \nabla \log Z(t, x))) + \frac{\sigma^2}{2} \nabla^2 \mu(t, x), \quad (12a)$$

$$\partial_t Z(t, x) = -H(\mu(t, x), Z(t, x)) + G(\mu(t, x), Z(t, x), r(x)) + D\sigma^2 \nabla^2 Z(t, x), \quad (12b)$$

where  $\mu(t, x) \in \mathbb{R}_{\geq 0}$  denotes the agents density,  $Z(t, x) \in \mathbb{R}_{\geq 0}$  denotes the intrinsic cue concentration, and  $r(x) \in \mathbb{R}$  denotes the extrinsic cue concentration. The parameter  $\sigma \in \mathbb{R}_{\geq 0}$  denotes the randomness of the agents' motility, determined by the scaling of time and space. The function  $\psi(\nabla Z, \nabla \log Z)$  represents the chemotactic response of the agents to the intrinsic cue concentration,  $H(\mu, Z)$  represents the degradation of the intrinsic cue by the agents, and  $G(\mu, Z, r)$  represents the production of the intrinsic cue by the agents. For the log-exp coupling model (6), (8), these functions are defined as:

$$\psi(\nabla Z, \nabla \log Z) = \gamma \sigma^2 \nabla \log Z, \quad H(\mu, Z) = \alpha \mu Z, \quad G(\mu, Z, r) = \alpha \mu \exp(\beta r) Z^\gamma. \quad (13)$$

This model is indeed composed of logarithmic gradient sensing  $\psi$  and intrinsic cue production  $G$  exponentially dependent on extrinsic cue concentration  $r$ . For the lin-lin coupling model (9), (10), the function are defined as:

$$\psi(\nabla Z, \nabla \log Z) = \gamma \sigma^2 \nabla Z, \quad H(\mu, Z) = \alpha(1 - \gamma) \mu Z, \quad G(\mu, Z, r) = \alpha \beta \mu r \quad (14)$$

This model is indeed composed of linear gradient sensing  $\psi$  and intrinsic cue production  $G$  linearly dependent on extrinsic cue concentration  $r$ .

Remarkably, the learning models have a structure homologous to the Keller-Segel models [38, 39], which was firstly introduced to model microbial populations that migrate while degrading intrinsic cue (attractant),

$$\partial_t n(t, x) = -\nabla \cdot (\chi n(t, x) \nabla \log s(t, x)) + D_n \nabla^2 n(t, x), \quad (15a)$$

$$\partial_t s(t, x) = -\kappa s(t, x) - \eta n(t, x) s(t, x) + D_s \nabla^2 s(t, x), \quad (15b)$$

where  $n(t, x)$  denotes the microbial density and  $s(t, x)$  denotes the intrinsic cue concentration.  $\chi \in \mathbb{R}$  represents the chemotaxis coefficient,  $D_n \in \mathbb{R}_{\geq 0}$  represents the randomness of the microbes,  $\kappa \in \mathbb{R}_{\geq 0}$  represents the decay constant of the intrinsic cue,  $\eta \in \mathbb{R}_{\geq 0}$  represents the degradation rate constant of the intrinsic cue by the cells, and  $D_s \in \mathbb{R}_{\geq 0}$  represents the diffusion coefficient of the intrinsic cue.

Comparing with the microbial migration equation (15a), one sees that the agent migration equation (12a) reproduces the phenomenological model. The randomness of the agents' motility in both the log-exp coupling model and the lin-lin coupling model corresponds to the microbial one ( $\sigma^2/2 = D_s$ ). Furthermore, for the log-exp coupling model (13), since  $\psi$  is proportional to the logarithmic gradient of the intrinsic cue, the gradient response term also corresponds completely to the microbial one ( $\chi = \gamma\sigma^2$ ). While many collective chemotaxis models use logarithmic gradient sensing, it has been experimentally reported that in bacterial chemotaxis, the response to the gradient varies between logarithmic gradient sensing and linear gradient sensing depending on the intrinsic cue [10, 11]. Thus, the lin-lin coupling model (14), which shows linear gradient sensing, can be regarded as a model for low concentration. Therefore, the policies (6), (9) in the learning models are the discrete version of the well-known collective chemotaxis models.

Comparing the intrinsic cue concentration equations (15b), (12b) not only reproduce the phenomenological model, but also elucidate a specific expression that were phenomenologically unaddressed. Both the log-exp coupling model and the lin-lin coupling model correspond to the microbial one in terms of the diffusion term ( $D\sigma^2/2 = D_n$ ), and the degradation term  $H$  ( $\alpha = \eta$  for the log-exp coupling model (13) and  $\alpha(1 - \gamma) = \eta$  for the lin-lin coupling model (14)) when  $\kappa \approx 0$ . Though the production term is not included in the classical Keller-Segel model (15), the term of the lin-lin coupling model (14) corresponds to the term of the extended models [26, 28], which heuristically incorporate intrinsic cue production by cells at a rate linearly dependent on the extrinsic cue but independent of the concentration. The linear production term of the lin-lin coupling model (14) optimally couples to linear gradient sensing, not to logarithmic gradient sensing. The production term optimally couples to logarithmic gradient sensing is the one of the log-exp coupling model (13), where the production rate depends exponentially on the extrinsic cue and on the intrinsic cue concentration, though this form of equation have been yet unaddressed by phenomenology alone.

As discussed above, the optimal couplings of gradient sensing and gradient generation based on the different mappings  $\mathcal{F}$  between state value and intrinsic cue concentration (log-exp coupling model and lin-lin coupling model) not only reproduce existing phenomenological models but also elucidate a specific expression that were previously unaddressed by phenomenology alone. What would be the behavior of cell populations with an inconsistent

|                                     |                                 | Keller-Segel              | log-exp model (13)                  | lin-lin model (14)             |
|-------------------------------------|---------------------------------|---------------------------|-------------------------------------|--------------------------------|
| Mapping from concentration to value | $\mathcal{F}[Z]$                | -                         | $\log(Z)/\beta$                     | $Z/\beta$                      |
| Chemotactic response                | $\psi(\nabla Z, \nabla \log Z)$ | $\chi \nabla \log Z$      | $\gamma \sigma^2 \nabla \log Z$     | $\gamma \sigma^2 \mu \nabla Z$ |
| Degradation                         | $H(\mu, Z)$                     | $(\eta \mu + \kappa)Z$    | $\alpha \mu Z$                      | $\alpha(1 - \gamma)\mu Z$      |
| Production                          | $G(\mu, Z, r)$                  | (in extensions, $\mu r$ ) | $\alpha \mu \exp(\beta r) Z^\gamma$ | $\alpha \beta \mu r$           |

TABLE I. Comparison of the continuous limits of the two learning models (12) with the classical Keller-Segel equation (15) for each component: the mapping  $\mathcal{F}[Z]$  from intrinsic cue concentration to the estimated state value, the chemotactic response  $\psi(\nabla Z, \nabla \log Z)$  to intrinsic cue concentration, degradation  $H(\mu, Z)$  of intrinsic cue, and production  $G(\mu, Z, r)$  of intrinsic cue. Phenomological parameters: chemotactic coefficient  $\chi$ , cellular degradation rate  $\eta$  and decay rate of the  $\kappa$ . Computational parameters: inverse control weight  $\beta$ , discount factor  $\gamma$ , agents' motility  $\sigma$  and learning rate  $\alpha$ .

coupling of gradient sensing and gradient generation, which is neither the log-exp coupling model nor the lin-lin coupling model? Would it still be optimal in terms of maximizing the cumulative regularized reward  $\mathcal{J}$  (1)? In the following sections IV A and IV B, we examine the importance of the optimal coupling of gradient sensing and gradient generation in achieving optimal migration through numerical experiments.

#### IV. NUMERICAL EXPERIMENTS

In this section, we conduct numerical experiments on learning models to evaluate their performance in a biological problem.

##### A. Demonstration through maze-solving

Exploration problems in complex environments, such as the accumulation of neutrophils at infected tissues [27] or the germ cell migration in embryos [40] are widely observed in biological systems. These problems can be interpreted as maze-solving, with various cells experimentally shown to navigate artificial mazes [6, 41]. In this section, we demonstrate the dynamics of learning models through a complex maze example. For the following numerical

experiments, we adapt a lazy random walk, similarly to Section III, with  $p(s|s) = \varepsilon$  and  $p(s'|s) = (1 - \varepsilon)/|\mathcal{N}(s)|$ , where  $s' \in \mathcal{N}(s)$ . The parameter  $\varepsilon \in [0, 1]$  represents the slowness of migration, reflecting that the migration speed varies across species, even in the same geometry [6]. We consider a complex maze environment with  $|\mathcal{S}| = 274$  vertices, modeled after the experiment [6, Figure 6], with the target only at the vertex  $s^{\text{goal}}$ . Initially, the intrinsic cue is uniformly distributed ( $Z_0(s) = Z_0$  for  $s \in \mathcal{S}$ ), and agents start exploring from vertex  $s_t^i = s^{\text{start}} \in \mathcal{S}$ . Agents modify the intrinsic cue concentration to reach the goal  $s^{\text{goal}} \in \mathcal{S}$  (Figure 3).

As a demonstration, we show snapshots of the concentration distribution  $Z_t$ , agent distribution  $\mu_t$ , and the time average regularized reward distribution  $(R^i[s_{0:t}^i, \pi_{0:t-1}])_{i=1}^N$  for one trial. The agent distribution  $\mu_t : \mathcal{S} \rightarrow \{0, 1, \dots, N\}$  is defined as  $\mu_t(s) := \sum_{i=1}^N \mathbb{1}_{s_t^i=s}$ . The time average regularized reward  $R^i[s_{0:T}^i, \pi_{0:T-1}]$  for agent  $i$  at time  $t$  is defined as:

$$R^i[s_{0:T}^i, \pi_{0:T-1}] := \frac{1}{T} \sum_{t'=0}^{T-1} \left( r(s_{t'}^i) - \frac{1}{\beta} \log \frac{\pi_{t'}(s_{t'+1}^i | s_{t'}^i)}{p(s_{t'+1}^i | s_{t'}^i)} \right), \quad (16)$$

which represents the cumulative extrinsic cue concentration sensed and motility control cost incurred by agent  $i$  from the start to time  $T$ , evaluating the state history. If the policy sequences  $\pi_{0:T-1}$  generating the trajectory  $s_{0:T}^i$  converges to the optimal policy in a sense of time average reward,  $\lim_{T \rightarrow \infty} R^i[s_{0:T}^i, \pi_{0:T-1}] = \lim_{\gamma \nearrow 1} (1 - \gamma) \max_{\pi} \mathcal{J}[\pi]$  (c.f. [42]), indicating that  $R^i[s_{0:T}^i, \pi_{0:T-1}]$  is related to the original optimization metric  $\mathcal{J}$  (1).

With the optimal coupling of the policy and update, namely the log-exp coupling model (6), (8), agents disperse at branching vertices, degrade the intrinsic cue, generate gradients toward unexplored directions, and expand their exploration area (Figure 3  $t = 21, 1001$ ). Upon reaching the goal, they produce the intrinsic cue, reinforcing the gradient toward the goal. Eventually, the gradient aligns from start to goal and many agents accumulate near the goal (Figure 3  $t = 15001$ ). Thus, the log-exp coupling model exhibits behaviors consistent with experimentally observed phenomena, such as exploration involving intrinsic cue degradation [4], and recruitment and target accumulation through intrinsic cue production [5]. As a result, even in complex environment, agents accumulate at the target through the intrinsic cue production and degradation, leading to higher  $R^i$  for many agents (Figure 3 (b), (c)  $t = 15001$ ). Similar behavior is observed in the optimal lin-lin coupling model (9), (10) (Figure S1).

However, agent population with non-optimal couplings of policy and update sometimes

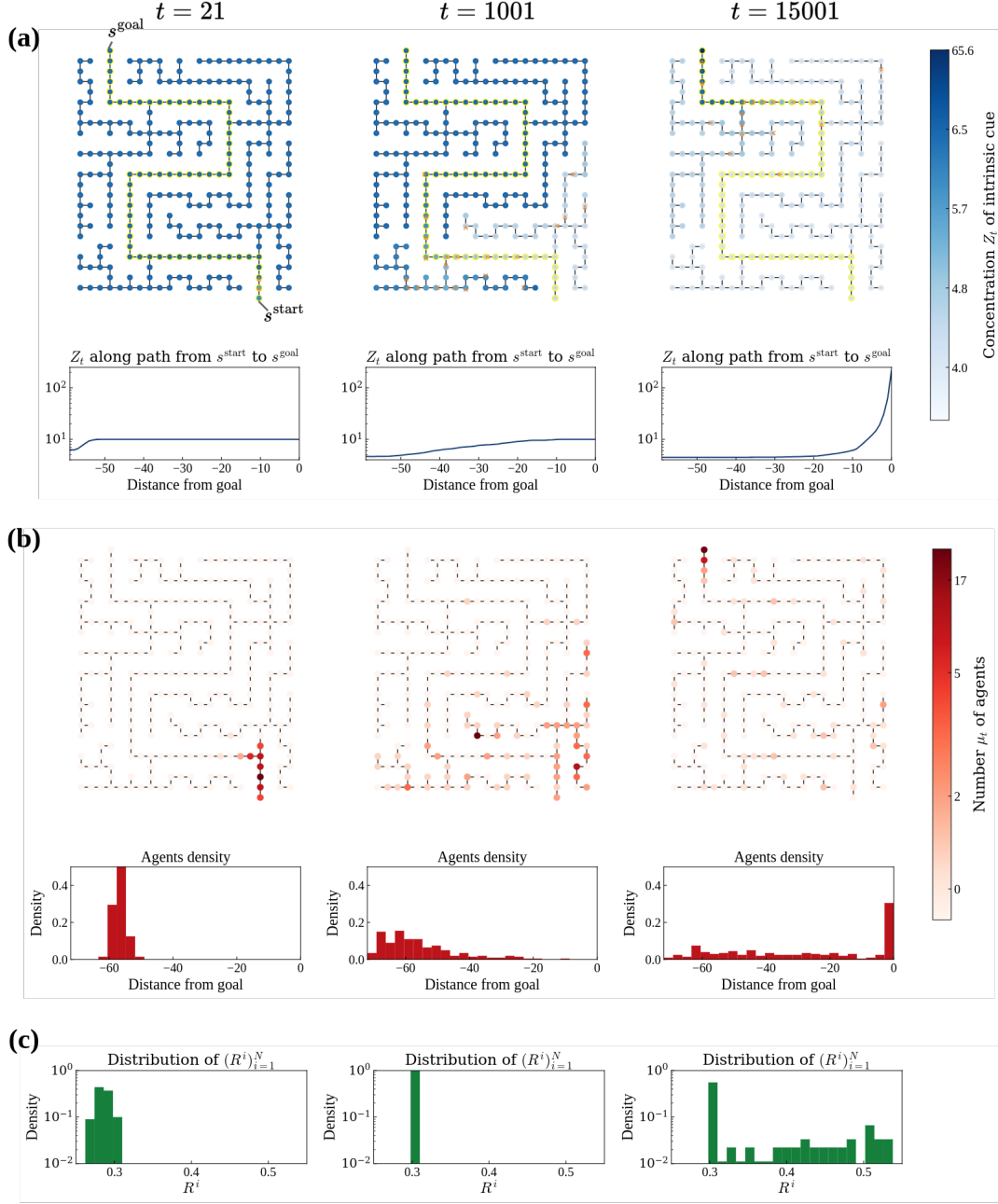


FIG. 3. Snapshots of one trial at  $t = 21, 1001, 15001$  evolved according to the optimal log-exp coupling model (6), (8). (a) Intrinsic cue concentration  $Z_t$ , (b) Agent distribution  $\mu_t$ , (c) The time average regularized reward distribution  $(R^i[s_{0:t}^i, \pi_{0:t-1}])_{i=1}^N$ . In (a) and (b), graphs are colored by the values at the vertices. Arrows in graphs of (a) indicate the gradient direction. Below graph of (a), the values are plotted along the shortest path (in yellow) against the distance from the goal. Below graphs of (b), agent distribution relative to the distance to the goal.  $\alpha = 0.0098$ ,  $N = 100$ ,  $D = 0.01$ ,  $\gamma = 0.8$ ,  $Z_0 = 10.0$ ,  $\varepsilon = 0.5$ ,  $\beta$ ,  $r(s^{\text{goal}}) = 1.5$ ,  $r(s) = 0.3$  for  $s \neq s^{\text{goal}}$ .

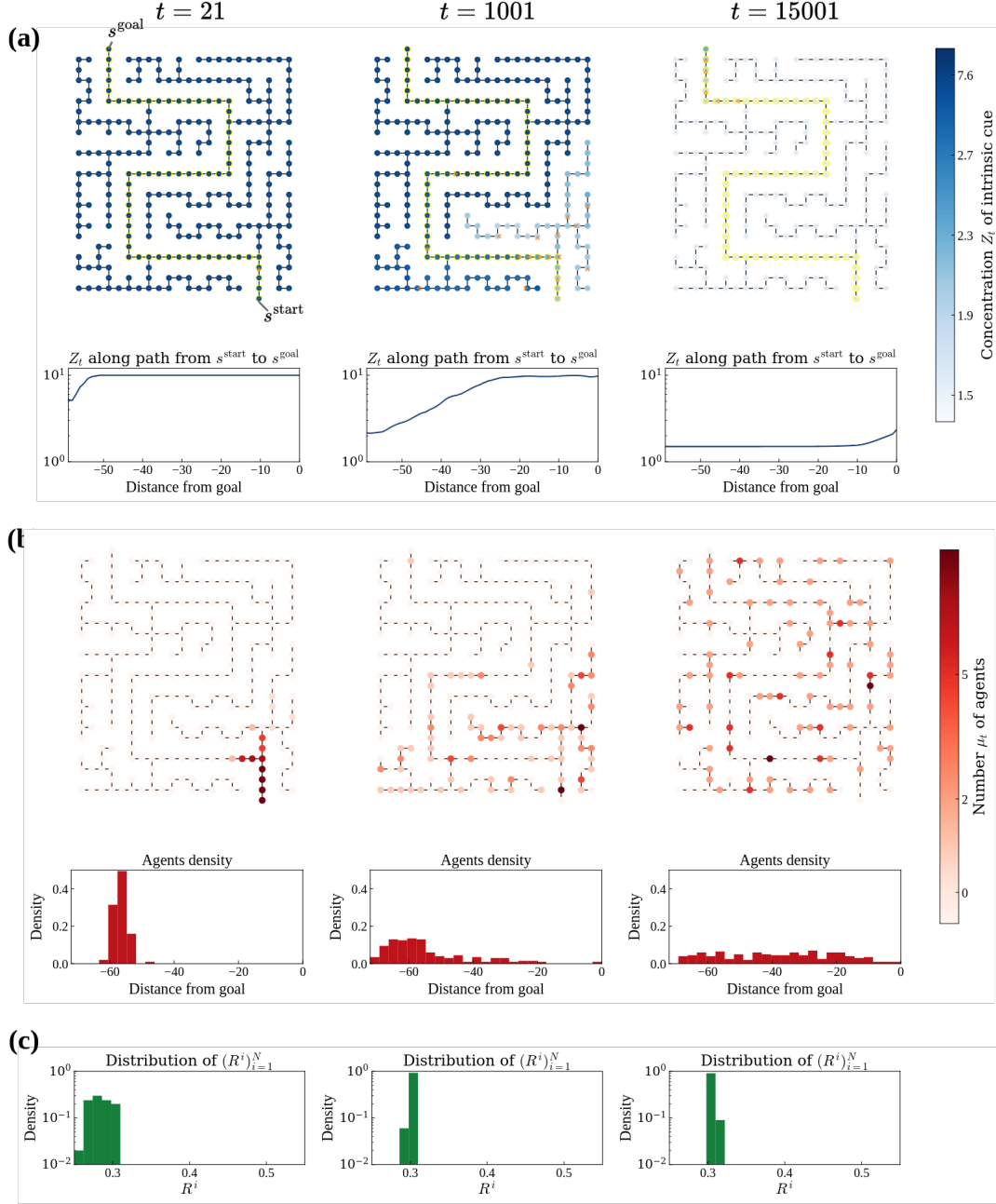


FIG. 4. Snapshots of one trial at  $t = 21, 1001, 15001$  evolved according to the non-optimal coupling (6), (10). (a) Intrinsic cue concentration  $Z_t$ , (b) Agent distribution  $\mu_t$ , (c) The time average regularized reward distribution  $(R^i[s_{0:t}^i, \pi_{0:t-1}])_{i=1}^N$ . In (a) and (b), graphs are colored by the values at the vertices. Arrows in graphs of (a) indicate the gradient direction. Below graph of (a), the values are plotted along the shortest path (in yellow) against the distance from the goal. Below graphs of (b), agent distribution relative to the distance to the goal.  $\alpha = 0.0098$ ,  $N = 100$ ,  $D = 0.01$ ,  $\gamma = 0.8$ ,  $Z_0 = 10.0$ ,  $\varepsilon = 0.5$ ,  $\beta$ ,  $r(s^{\text{goal}}) = 1.5$ ,  $r(s) = 0.3$  for  $s \neq s^{\text{goal}}$ .

fail to accumulate at the target even under conditions similar to Figure 3. With a non-optimal coupling of a logarithmic sensing policy (6) and a linear producing update (9), agents disperse, degrade the intrinsic cue and generates a concentration field with higher concentrations closer to the target, similarly to Figure 3. However, they generate a shallow gradient, and even as the concentration approaches steady state, most agents fail to accumulate at the target, resulting in low  $R^i$  for most agents (Figure 4  $t = 15001$ ). This suggests that a logarithmic sensing policy (6) and a linear producing update (9) is a non-optimal coupling. Another non-optimal coupling of linear sensing policy (9) and exponentially producing update (8) shows overaccumulation instead of dispersion (Appendix. C 1).

## B. Optimality evaluation

In this section, we investigate the optimality of the couplings, demonstrated in Sec. IV A, by comparing the steady states, each consisting of a policy (6) or (9) and an update (8) or (10). As the simplest environment for theoretical comparison, we consider a graph with 20 vertices  $\mathcal{S} = \{s^0, s^1, \dots, s^{19}\}$  connected in a chain, where a target locates at vertex  $s^{19}$  (Figure 5 (a)).

At the almost steady states, the concentration  $Z_T$  qualitatively differ depending on both the update and the policy (Figure 5 (b)). The linearly producing update (10) generate similarly gradual distributions  $Z_T$ , whether coupled with the optimal linear sensing policy (9) or the non-optimal logarithmic sensing policy (6), with little  $\beta$  dependence. In contrast, the exponentially producing update (8) generates a steep  $Z_T$  with the optimal logarithmic sensing policy (6), whereas it generates a uniformly high, gradual distribution with the non-optimal linear sensing policy (9) if  $\beta$  is sufficiently high, indicating a low control cost (Figure 5 (b)  $\beta = 1.5$ ). The steady agent distributions  $\mu_T$  are nearly identical for the optimal couplings (log-exp and lin-lin) with each  $\beta$ , while for the non-optimal couplings, they either aggregate at the target or disperse (Figure 5 (c)). For the optimal couplings, agents accumulate more at the target as  $\beta$  increases, indicating lower control cost. For the non-optimal coupling (log-lin), the distribution shows little  $\beta$  dependence and remains dispersed, corresponding to Figure 4 (b). For the non-optimal coupling (lin-exp), agents aggregate at the target when  $\beta$  is sufficiently high.

These observations can be qualitatively understood: for low intrinsic cue concentrations,

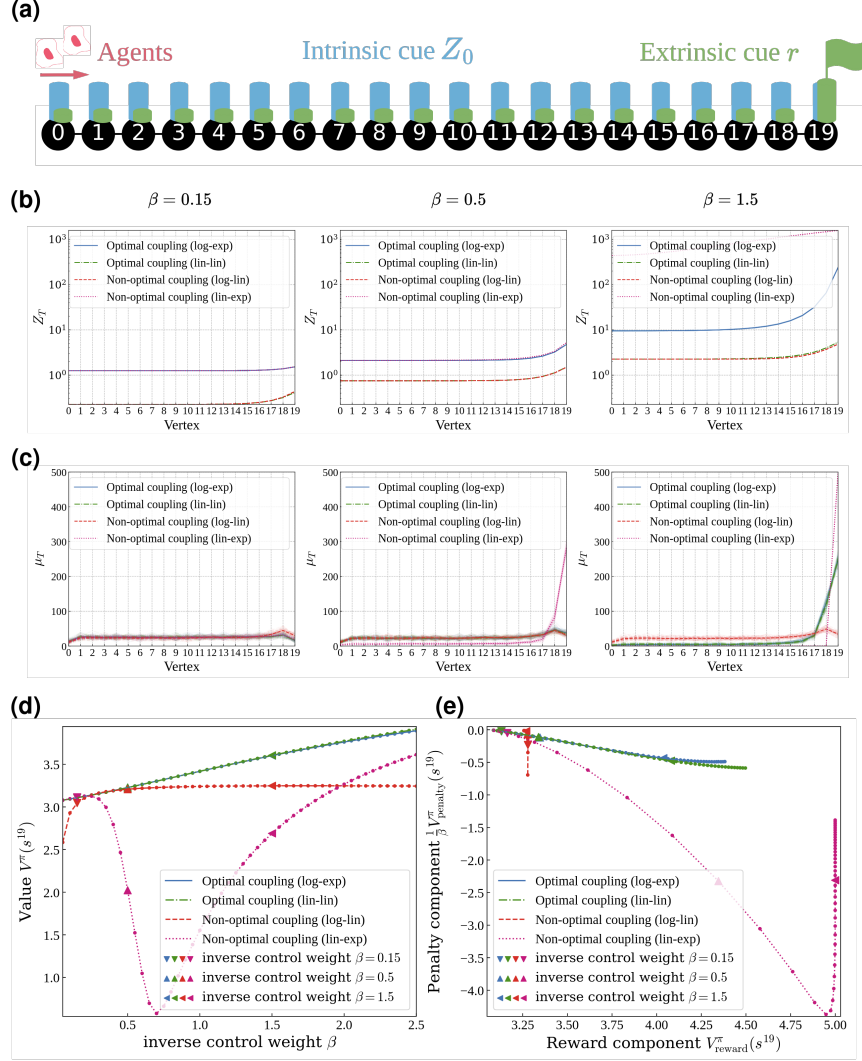


FIG. 5. (a) A graph with 20 vertices  $\{s^0, s^1, \dots, s^{19}\}$  connected in a chain, shown with the initial condition. The target is located only at vertex  $s^{19}$ :  $r(s^{19}) = 1.0$  and  $r(s) = 0.3$  for  $s \neq s^{19}$ . (b) Intrinsic cue concentration  $Z_T$  and (c) Agent distribution  $\mu_T$  at  $T = 8000$  for 50 trials with  $\beta \in \{0.15, 0.5, 1.5\}$  for optimal and non-optimal couplings. Optimal coupling (log-exp): Eqs. (6), (8); Optimal coupling (lin-lin): Eqs. (9), (10); Non-optimal coupling (log-lin): Eqs. (6), (8); and Non-optimal coupling (lin-exp): Eqs. (9), (10). Each trial's  $Z_T$  and  $\mu_T$  are shown with thin solid lines and the trial averages  $\tilde{Z}_T$ ,  $\tilde{\mu}_T$  are shown with thick solid lines. (d) State value  $V^\pi(s^{19})$  at vertex  $s^{19}$  for each policy  $\pi[\tilde{Z}_T]$  based on the trial-averaged steady concentration  $\tilde{Z}_T$  for the four couplings with  $\beta \in [0.25, 2.5]$ . (e) The relationship between the reward component  $V_{\text{reward}}^\pi(s^{19})$  and penalty component  $\frac{1}{\beta} V_{\text{penalty}}^\pi(s^{19})$  of  $V^\pi(s^{19})$  for the four couplings with  $\beta \in [0.25, 2.5]$ .  $N = 500$ ,  $\varepsilon = 0.5$ ,  $\alpha = 0.00196$ ,  $D = 0.01$ ,  $\gamma = 0.8$ ,  $\beta \in [0.25, 2.65]$ .

the logarithmic sensing policy (6) responds more strongly than the linear sensing policy (9). For sufficiently high concentrations, the logarithmic sensing policy (6) responds more weakly than the linear sensing policy (9). Additionally, the exponentially producing update (8) generates a steeper concentration distribution compared to the linearly producing update (10). As a result, for the non-optimal coupling (log-lin), the logarithmic sensing policy (6) underestimates the gradual concentration gradient generated by the linearly producing update (10), making it relatively easier to accumulate near the target when the concentration is low and harder when it is high. In contrast, for the non-optimal coupling (lin-exp), the linear sensing policy (6) overestimates the gradient generated by the exponentially producing update (8), making it easier to accumulate near the target as the concentration is higher, indicating a lower control cost.

To evaluate the qualitative observations on the optimality of the steady states, we fix the concentration to the trial-averaged steady concentration  $\tilde{Z}_T$  and examine the state value function  $V^\pi$  (3) for each policy  $\pi[\tilde{Z}_T]$  (6) or (9), along with the reward component  $V_{\text{reward}}^\pi$  and the penalty (control cost) component  $V_{\text{penalty}}^\pi$  ( $V^\pi = V_{\text{reward}}^\pi + V_{\text{penalty}}^\pi/\beta$ ).

$$V_{\text{reward}}^\pi(s) := E \left[ \sum_{t=0}^{\infty} \gamma^t r(s_t) \middle| s_0 = s \right] \quad s \in \mathcal{S}, \quad (17a)$$

$$V_{\text{penalty}}^\pi(s) := -E \left[ \sum_{t=0}^{\infty} \gamma^t \log \frac{\pi(s_{t+1}|s_t)}{p(s_{t+1}|s_t)} \middle| s_0 = s \right] \quad s \in \mathcal{S}. \quad (17b)$$

These values are obtained by value iteration method (Appendix. A 2), and additional state values are provided in Figure S3.

The state value  $V^\pi$ , the optimization metric, is larger for the optimal couplings (log-exp and lin-lin) than for the non-optimal couplings (log-lin and lin-exp) for any  $\beta$ . The reward component  $V_{\text{reward}}^\pi$  and the penalty component  $V_{\text{penalty}}^\pi(s^{19})/\beta$  of  $V^\pi$  are better balanced for the optimal couplings. Both optimal couplings (log-exp and lin-lin) show an increase in  $V^\pi$  with larger  $\beta$  (Figure 5(d)), and a trade-off between  $V_{\text{reward}}^\pi$  and  $V_{\text{penalty}}^\pi/\beta$  with larger  $\beta$  (Figure 5(e)). Despite the difference shapes of  $\tilde{Z}_T$  (Figure 5(b)), the two optimal couplings exhibit almost identical balances of  $V_{\text{reward}}^\pi$  and  $V_{\text{penalty}}^\pi/\beta$ . However, for the non-optimal coupling (log-lin),  $V_{\text{reward}}^\pi$  remains constant regardless of  $\beta$ , while the absolute value of  $V_{\text{penalty}}^\pi/\beta$  is larger for smaller  $\beta$ , indicating higher control costs (Figure 5(e)), resulting in a smaller total  $V^\pi$  (Figure 5(d)). For the non-optimal coupling (lin-exp), although  $V_{\text{reward}}^\pi$  is higher for larger  $\beta$ , the absolute value of  $V_{\text{penalty}}^\pi/\beta$ , which dominates the total  $V^\pi$ , increases up to

$\beta \approx 0.7$ , resulting in a decrease in  $V^\pi$  up to  $\beta \approx 0.7$  (Figure 5(d)). Consequently, agents' dispersion and overaccumulation in  $\mu_T$  of the non-optimal couplings are characterized by imbalance between  $V_{\text{reward}}^\pi$  and  $V_{\text{penalty}}^\pi/\beta$ , resulting in smaller  $V^\pi$  than that of the optimal couplings. This suggests that non-optimal couplings are indeed non-optimal in terms of the optimization problem (4) for accumulating at the targets.

These results highlight that the optimal intrinsic cue production required for optimal migration qualitatively differs depending on the sensing characteristics: the logarithmic sensing policy optimally couples to the production exponentially dependent on extrinsic cue concentration, whereas the linear gradient sensing policy optimally couples to the production linearly dependent on the concentration. Nonetheless, there is no difference between the two optimal couplings in terms of the optimization criterion. To determine which is superior, it is necessary to discuss the biological aspects, such as the cellular gradient sensing characteristics and the shape of the steady-state concentration gradient generated by the cells.

### C. Comparison with a single-agent system

We previously analyzed distributed learning models where agents with limited memory disperses and cooperatively learns environmental information through the environment, focussing on collective chemotaxis models. In contrast, higher organisms store environmental information within each individual's internal model, like the brain, and adaptively change the models to learn behaviors [43]. What are the advantages and disadvantages of the unsmart agent population compared to the structurally different information processing system of a smart single agent, a long-standing subject of reinforcement learning theory? Even if both systems achieve the same objective, metrics such as robustness during the learning process depend on the system's structure, and their comparative advantages can vary based on these metrics [44] (c.f. No free lunch theorem for search [45]). In this section, comparing the learning processes of both systems with the same objective, we investigate the functional role of the distributive structure in information processing.

Specifically, we consider a single agent with a state  $s_t \in \mathcal{S}$  and an estimated state value function  $Z_t : \mathcal{S} \rightarrow \mathbb{R}_{\geq 0}$  as internal memory at each time step  $t = 0, 1, \dots$ . The agent transitions its state based on  $Z_t$  following the same policy (6) as log-exp coupling model,

and an update nearly identical to update (8) as follows:

$$Z_{t+1}(s) - Z_t(s) = -\mathbb{1}_{s_t=s}\alpha'\Delta Z_t(s). \tag{18}$$

The intrinsic cue diffusion term (8b) included in the agent population’s update (8) is absent in the single agent’s learning (18), where  $Z_t$  is retained as internal memory. Thus, the update is identical to the standard greedy Z-learning [33]. For comparison, the learning rate  $\alpha' \in (0, 1)$  for the single agent is set to  $\alpha' = \alpha N$ , indicating that it has the same learning capability as the entire agent population.

The single agent explores while updating  $Z_t$  similarly to the agent population. The update magnitude at each vertex is larger, but the overall update speed of  $Z_t$  is slower due to the limited exploration range. (Figure 6(a)  $t = 1001$ ). At a time  $t = 15001$ , where the agent population has mostly completed learning and some agents have accumulated at the target (Figure 3 (a) (b)), the single agent may not have progressed, thus not accumulating at the target. Additionally, without diffusion in the value update, the value distribution, which should increase monotonically from the start to the goal in an optimality, becomes irregular due to random stay histories (Figure 6(a)  $t = 1001$ ). This one-trial comparison suggests that the smart single agent may not explore and learn as effectively as the unsmart agent population, failing to accumulate at the target.

Multiple trials provide a more quantitative evaluation. First, we compared the first hitting time  $k^i[s_{0:T}^i]$  to the goal for both the agent population and the single agent, where  $k^i[s_{0:T}^i] = \min\{t \in \{1, 2, \dots, T\} | s_t^i = s^{\text{goal}}\}$  if  $s^{\text{goal}} \in \{s_t^i\}_{t=0:T}$  and  $k^i[s_{0:T}^i] = T$  otherwise. While some agents in the population sometimes reach the goal slower, a portion of the population can reach the goal faster than the single agent, by dispersion (Figure 6 (b)). Next, we evaluate the performance of the learning process using the time average regularized reward  $R^i$  (16), related to the optimization metric  $\mathcal{J}$  (1) (Figure 6 (c)). The bottom 50%  $R^i$  of the agent population is smaller than the median of the single agents’ trial, corresponding to agents that happen to wander into dead ends and get left behind (Figure 3 (b)  $t = 15001$ ). However, the top 20%  $R^i$  of the agent population for 80% of trials are larger than the top 30% of the single agent’s trials. These comparisons of multiple trials indicates that the smart single agent, which retains environmental information as complete internal memory and concentrates its memory update resources, has a lower probability of goal accumulation compared to the entire unsmart agent population, which disperses and shares

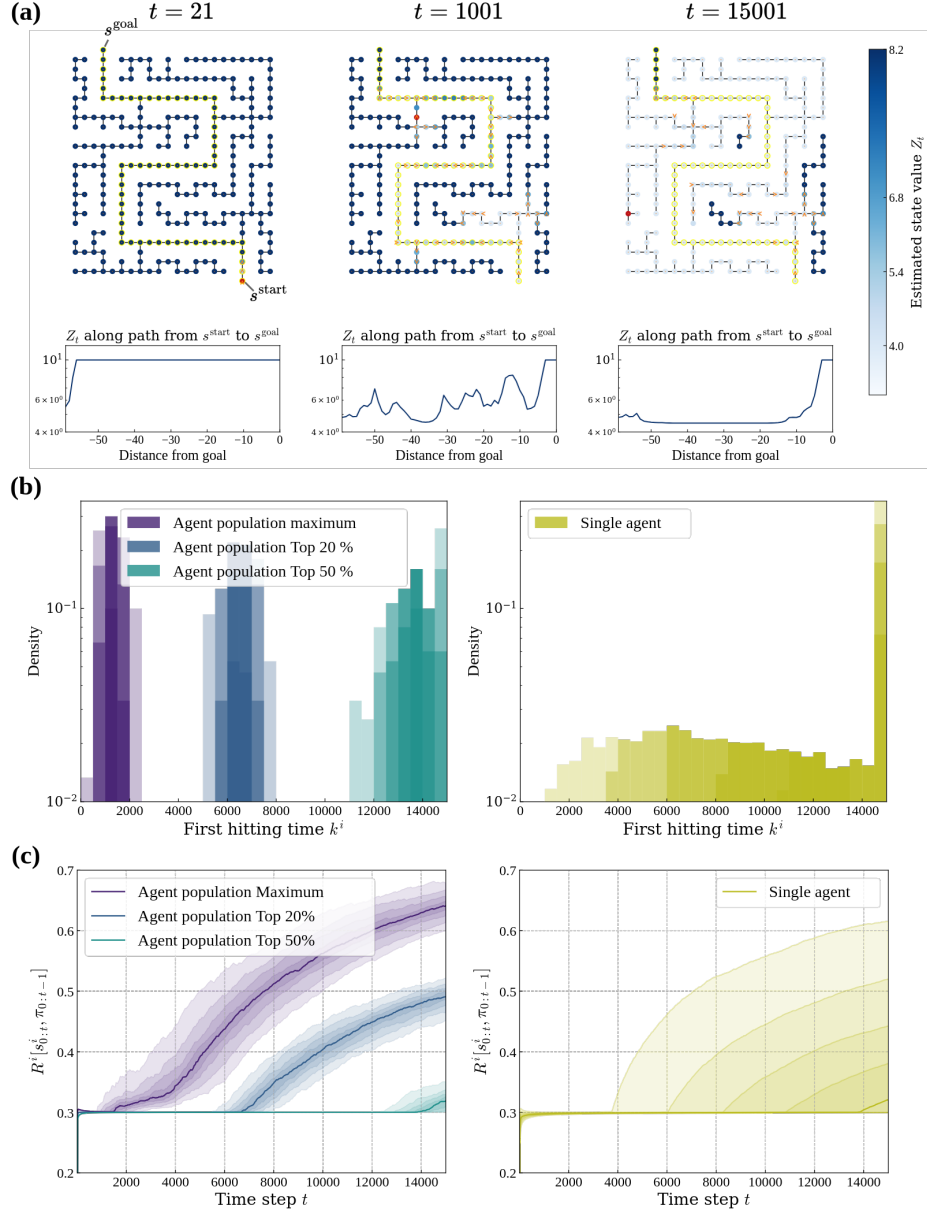


FIG. 6. (a) snapshots of the estimated state value  $Z_t$  at  $t = 21, 1001, 15001$  for one trial for a single agent following a policy (6), update (18). The graph is colored by vertex values, with arrows indicating the gradient direction. Below the graph, a plot shows values along the path (highlighted in yellow) against the distance from the start point. Vertices where the agent is located are marked in red. (b) Distribution of the first hitting time  $k^i[s_{0:T}^i]$  to  $s^{\text{goal}}$  for 150 of the unsmart agent population and 15000 trials of the smart single agent. For the single agent, the first hitting time is represented with overlapping color bands from the median to the maximum and minimum values in 10% increments. (c) Time variation of the time average regularized reward  $R^i[s_{0:t}^i, \pi_{0:t-1}]$  for each agent in the population and the single agent. Each solid line represents the maximum, top 20%, and top 50% within the agent population, as well as the median value for the smart single agent. Shaded bands indicate the range from the 10th to the 90th percentile in 10% increments. Agent population:  $(\alpha, N, D) = (0.0098, 100, 0.01)$ , smart single agent:  $(\alpha, N, D) = (0.98, 1, 0)$ . The number of trials: 150 for the agent population and 15000 for the single agent.  $\gamma = 0.8$ ,  $Z_0 = 10.0$ ,  $\varepsilon = 0.5$ ,  $\beta = 1.0$ ,  $r(s^{\text{goal}}) = 1.5$ ,  $r(s) = 0.3$  for  $s \neq s^{\text{goal}}$ .

information through the environment. Therefore, the agent population might function not only to primarily accumulate at the goal (1) but also to secondarily ensure a portion of the population robustly achieves this primary function. In real biological problems such as the neutrophil accumulation at a wound site, prioritizing the rapid arrival of a portion of the population over the entire population is effective against exponentially growing pathogens entering from the wound.

## V. DISCUSSION

### A. Conclusion

In this paper, we clarified the optimal coupling between concentration gradient responses and concentration generation by formulating a cell population that shares environmental information via attractants in the environment as a distributed reinforcement learning agent population. Specifically, by associating the state value in reinforcement learning (i.e., the likelihood of accumulating at target) with the attractant concentration in the environment, we interpreted the process where individual cells produce and degrade the attractant based on their local sensing as the process where an agent population learns the optimal state value in a distributed manner. We derived two qualitatively different optimal couplings between concentration gradient responses and concentration generation, depending on whether the response to the gradient is linear or logarithmic. The derived dynamics has a continuous limit homogeneous to the Keller-Segel model, suggesting that cell populations might engage in learning. Also, numerical experiments confirmed the importance of optimality in couplings between sensing and production. Furthermore, by comparing with a smart single agent possessing complete internal memory, we demonstrated that the unsmart agent population, learning in a distributed manner via external attractants, has the function of stabilizing the learning process. Our results provide a foundation for quantitatively understanding the information processing mediated by extracellular signals.

### B. Discussion

Experiments have shown that the gradient sensing in bacterial chemotaxis vary between linear and logarithmic depending on the attractant concentration [10, 11]. We computation-

ally demonstrate using entropy-regularized reinforcement learning theory that the optimal gradient sensing can also vary between linear and logarithmic, depending on whether attractant production by agents is linear or exponential with respect to target information. By leveraging the log in KL divergence, we introduced a logarithmic mapping between state value and concentration,  $\mathcal{F}[Z_t] = \log Z_t/\beta$ . It is also possible to introduce other nonlinear mapping  $\mathcal{F}$  using different relative entropies (e.g., Tsallis relative entropy) and discuss the corresponding gradient sensings and concentration field generations. For simplicity, this paper focuses on cases where the attractant degradation depends linearly on the number of cells and the attractant concentration, leading to two learning models with different attractant production characteristics (8c), (10b). By applying other nonlinear transformations to the theoretical core, the Bellman optimality equation (S10), (S13c), one can derive more general forms of concentration field generation that include nonlinear attractant degradation, discussing the optimal coupling with gradient sensings.

The attractant diffusivity was interpreted as a physical constraint and added to the cost as Dirichlet energy in the main text, however, it can also be computationally interpreted as regularization that ensures continuous values between adjacent vertices in the graph [46]. While we introduced Laplacian regularization to ensure smooth values [47], the same argument applies to other regularizations. For example,  $L^2$  regularization ( $\lambda|Z_t|_2^2$ ,  $\lambda \in \mathbb{R}_{\geq 0}$ ) to prevent extreme values reducing large values, results in a sequential regularization term  $-\lambda Z_t(s)$ , which corresponds to the attractant decay ( $\lambda = \kappa$ , Eq. (15b)) in Keller-Segel type equations, or the evaporation of pheromones in ant dynamics[48]. It may also be worthwhile to extend the regularization to account for agent-dependent nonlinear diffusion, such as changes in the diffusivity of attractants due to enzymes produced by cells [49].

Understanding the collective information processing require discussing the functionality of its structure that includes agents, the population, and the environment, which is absent in single-agent information processing. We demonstrated that an unsmart agent population learning in a distributed manner via the external environment can robustly achieve a portion of agents accumulating at the target, compared to a single smart agent with complete internal memory. The phenomenon where the arrival time of the fastest individuals plays a more critical role than that of the population average is ubiquitous in biological phenomena, from synapses signaling to fertilization. It has been theoretically shown that having many particles with the same objective increases the probability of quickly achieving rare events,

known as the redundancy principle [50]. According to this principle, in cell populations with low replication costs, such as neutrophils, a structure that disperses a large number of genetically identical cells to maintain the population stably might be evolutionarily selected.

Moreover, the evolutionary selection of collective information processing structure involves not only the relationship between the collective and individuals but also their interaction with the external environment. This study demonstrated that the information-sharing via signaling molecules in the external environment, observed in cell populations, can be viewed as a reinforcement learning process where memory of target location is shared and cooperatively learned through modification of the molecule concentration. Achieving an optimal migration in the learning process requires the optimal coupling between individual gradient sensing and concentration field generation in the external environment. The argument that not only agents' internal traits but also action affecting the external environment are evolutionarily selected aligns with Dawkins' Extended Phenotype [51], which can be applied across various species.

In this study, for simplicity, we assumed that the reward function, which determines the agents' optimal behavior, depends only on targets' location and is expressed as a single extrinsic cue concentration. However, the optimal behavior might be influenced by integrated information from other agents mediated by various cues. In cellular populations, interactions between agents play crucial roles in biological functions. For example, responses are modulated by chemokines released by other immune cells to prevent inflammation [52], agents recognize and aggregate in response to the others' states to adapt to starvation [53], or agents repel each other to form tissues [54]. Therefore, extending the reinforcement learning problem to include reward functions dependent on the number of other agents [55] to discuss collective chemotaxis involving individual interactions is one future challenge. Another challenge is to explore the functionality of using multiple chemicals [56] by investigating learning dynamics involving multiple cues, including repellent.

This study assumed a homogeneous population where each individual follows the same behavior policy and update rule. However, biological functions often involve heterogeneous cell populations, such as leaders climbing gradients at the front and followers trailing behind [57]. Extending the learning problem to heterogeneous populations with different behavior policies and update policies [58] can investigate the relationship between heterogeneity and

collective function.

## ACKNOWLEDGMENTS

The first author received JSPS Research Fellowship Grant No.24KJ0846.

---

- [1] Shuvasree SenGupta, Carole A. Parent, and James E. Bear. The principles of directed cell migration. *Nature Reviews Molecular Cell Biology*, Vol. 22, No. 8, pp. 529–547, Aug 2021.
- [2] Andrew D Luster, Ronen Alon, and Ulrich H von Andrian. Immune cell migration in inflammation: present and future therapeutic targets. *Nature immunology*, Vol. 6, No. 12, pp. 1182–1190, 2005.
- [3] Peter Friedl and Darren Gilmour. Collective cell migration in morphogenesis, regeneration and cancer. *Nature reviews Molecular cell biology*, Vol. 10, No. 7, pp. 445–457, 2009.
- [4] Robert H. Insall, Peggy Paschke, and Luke Tweedy. Steering yourself by the bootstraps: how cells create their own gradients for chemotaxis. *Trends in Cell Biology*, Vol. 32, No. 7, pp. 585–596, Jul 2022.
- [5] Sofia De Oliveira, Emily E Rosowski, and Anna Huttenlocher. Neutrophil migration in infection and wound repair: going forward in reverse. *Nature Reviews Immunology*, Vol. 16, No. 6, pp. 378–391, 2016.
- [6] Luke Tweedy, Peter A. Thomason, Peggy I. Paschke, Kirsty Martin, Laura M. Machesky, Michele Zagnoni, and Robert H. Insall. Seeing around corners: Cells solve mazes and respond at a distance using attractant breakdown. *Science*, Vol. 369, No. 6507, p. eaay9792, 2020.
- [7] Béatrice Bréart, Willy D Ramos-Perez, Alejandra Mendoza, Abdelghaffar K Salous, Michael Gobert, Yong Huang, Ralf H Adams, Juan J Lafaille, Diana Escalante-Alcalde, Andrew J Morris, and Susan R Schwab. Lipid phosphate phosphatase 3 enables efficient thymic egress. *Journal of Experimental Medicine*, Vol. 208, No. 6, pp. 1267–1278, 2011.
- [8] Tim Lämmermann, Philippe V Afonso, Bastian R Angermann, Ji Ming Wang, Wolfgang Kastentmüller, Carole A Parent, and Ronald N Germain. Neutrophil swarms require ltb4 and integrins at sites of cell death in vivo. *Nature*, Vol. 498, No. 7454, pp. 371–375, 2013.
- [9] Olivia Susanto, Yvette WH Koh, Nick Morrice, Sergey Tumanov, Peter A Thomason, Matthew

- Nielson, Luke Tweedy, Andrew J Muinonen-Martin, Jurre J Kamphorst, Gillian M. Mackay, and Robert H. Insall. Lpp3 mediates self-generation of chemotactic lpa gradients by melanoma cells. Journal of cell science, Vol. 130, No. 20, pp. 3455–3466, 10 2017.
- [10] Yevgeniy V Kalinin, Lili Jiang, Yuhai Tu, and Mingming Wu. Logarithmic sensing in escherichia coli bacterial chemotaxis. Biophysical journal, Vol. 96, No. 6, pp. 2439–2448, 2009.
- [11] Milena D. Lazova, Tanvir Ahmed, Domenico Bellomo, Roman Stocker, and Thomas S. Shimizu. Response rescaling in bacterial chemotaxis. Proceedings of the National Academy of Sciences, Vol. 108, No. 33, pp. 13870–13875, 2011.
- [12] Yuhai Tu. Quantitative modeling of bacterial chemotaxis: signal amplification and accurate adaptation. Annual review of biophysics, Vol. 42, No. 1, pp. 337–359, 2013.
- [13] Antonio Celani and Massimo Vergassola. Bacterial strategies for chemotaxis response. Proceedings of the National Academy of Sciences, Vol. 107, No. 4, pp. 1391–1396, 2010.
- [14] HH Mattingly, K Kamino, BB Machta, and T Emonet. Escherichia coli chemotaxis is information limited. Nature physics, Vol. 17, No. 12, pp. 1426–1431, 2021.
- [15] Kento Nakamura and Tetsuya J. Kobayashi. Optimal sensing and control of run-and-tumble chemotaxis. Physical Review Research., Vol. 4, p. 013120, Feb 2022.
- [16] Ricard Alert, Alejandro Martínez-Calvo, and Sujit S. Datta. Cellular sensing governs the stability of chemotactic fronts. Phys. Rev. Lett., Vol. 128, p. 148101, Apr 2022.
- [17] Trung V Phan, Henry H Mattingly, Lam Vo, Jonathan S Marvin, Loren L Looger, and Thierry Emonet. Direct measurement of dynamic attractant gradients reveals breakdown of the patlak–keller–segel chemotaxis model. Proceedings of the National Academy of Sciences, Vol. 121, No. 3, p. e2309251121, 2024.
- [18] Xiongfei Fu, Setsu Kato, Junjiajia Long, Henry H Mattingly, Caiyun He, Dervis Can Vural, Steven W Zucker, and Thierry Emonet. Spatial self-organization resolves conflicts between individuality and collective migration. Nature communications, Vol. 9, No. 1, p. 2177, 2018.
- [19] Henry H Mattingly and Thierry Emonet. Collective behavior and nongenetic inheritance allow bacterial populations to adapt to changing environments. Proceedings of the National Academy of Sciences, Vol. 119, No. 26, p. e2117377119, 2022.
- [20] Brian A Camley. Collective gradient sensing and chemotaxis: modeling and recent developments. Journal of Physics: Condensed Matter, Vol. 30, No. 22, p. 223001, 2018.
- [21] David Ellison, Andrew Mugler, Matthew D Brennan, Sung Hoon Lee, Robert J Huebner,

- Elijah R Shamir, Laura A Woo, Joseph Kim, Patrick Amar, Ilya Nemenman, et al. Cell-cell communication enhances the capacity of cell ensembles to sense shallow gradients during morphogenesis. Proceedings of the National Academy of Sciences, Vol. 113, No. 6, pp. E679–E688, 2016.
- [22] Andrew Mugler, Andre Levchenko, and Ilya Nemenman. Limits to the precision of gradient sensing with spatial communication and temporal integration. Proceedings of the National Academy of Sciences, Vol. 113, No. 6, pp. E689–E695, 2016.
- [23] Sean Fancher and Andrew Mugler. Fundamental limits to collective concentration sensing in cell populations. Phys. Rev. Lett., Vol. 118, p. 078101, Feb 2017.
- [24] Jonas Cremer, Tomoya Honda, Ying Tang, Jerome Wong-Ng, Massimo Vergassola, and Terence Hwa. Chemotaxis as a navigation strategy to boost range expansion. Nature, Vol. 575, No. 7784, pp. 658–663, 2019.
- [25] David T Fraebel, Harry Mickalide, Diane Schnitkey, Jason Merritt, Thomas E Kuhlman, and Seppe Kuehn. Environment determines evolutionary trajectory in a constrained phenotypic space. Elife, Vol. 6, p. e24669, 2017.
- [26] Alberto Pezzotta, Matteo Adorisio, and Antonio Celani. Chemotaxis emerges as the optimal solution to cooperative search games. Physical Review E, Vol. 98, No. 4, Oct 2018.
- [27] Elzbieta Kolaczowska and Paul Kubes. Neutrophil recruitment and function in health and inflammation. Nature Reviews Immunology, Vol. 13, No. 3, pp. 159–175, 2013.
- [28] Alex C Szatmary, Ralph Nossal, Carole A Parent, and Ritankar Majumdar. Modeling neutrophil migration in dynamic chemoattractant gradients: assessing the role of exosomes during signal relay. Molecular biology of the cell, Vol. 28, No. 23, pp. 3457–3470, 2017.
- [29] Stefan Uderhardt, Andrew J Martins, John S Tsang, Tim Lämmermann, and Ronald N Germain. Resident macrophages cloak tissue microlesions to prevent neutrophil-driven inflammatory damage. Cell, Vol. 177, No. 3, pp. 541–555, 2019.
- [30] Lai Guan Ng, Jim S Qin, Ben Roediger, Yilin Wang, Rohit Jain, Lois L Cavanagh, Adrian L Smith, Cheryl A Jones, Michael De Veer, Michele A Grimbaldston, et al. Visualizing the neutrophil response to sterile tissue injury in mouse dermis reveals a three-phase cascade of events. Journal of Investigative Dermatology, Vol. 131, No. 10, pp. 2058–2068, 2011.
- [31] Philippe V Afonso, Mirkka Janka-Junttila, Young Jong Lee, Colin P McCann, Charlotte M Oliver, Khaled A Aamer, Wolfgang Losert, Marcus T Cicerone, and Carole A Parent. Ltb4 is

- a signal-relay molecule during neutrophil chemotaxis. Developmental cell, Vol. 22, No. 5, pp. 1079–1091, 2012.
- [32] Katharina M Glaser, Michael Mihlan, and Tim Lämmermann. Positive feedback amplification in swarming immune cell populations. Current Opinion in Cell Biology, Vol. 72, pp. 156–162, 2021.
- [33] Emanuel Todorov. Efficient computation of optimal actions. Proceedings of the National Academy of Sciences - PNAS, Vol. 106, No. 28, pp. 11478–11483, Jul 2009.
- [34] Andrew G. Barto and Richard S. Sutton. Reinforcement learning: an introduction. The MIT Press, 2018.
- [35] Doina Precup, Richard S. Sutton, and Satinder P. Singh. Eligibility traces for off-policy policy evaluation. In Proceedings of the Seventeenth International Conference on Machine Learning, ICML2000, pp. 759–766, San Francisco, CA, USA, 2000. Morgan Kaufmann Publishers Inc.
- [36] Volodymyr Mnih, Adria Puigdomenech Badia, Mehdi Mirza, Alex Graves, Timothy Lillicrap, Tim Harley, David Silver, and Koray Kavukcuoglu. Asynchronous methods for deep reinforcement learning. In Proceedings of The 33rd International Conference on Machine Learning, Vol. 48 of Proceedings of Machine Learning Research, pp. 1928–1937, New York, New York, USA, 20–22 Jun 2016. PMLR.
- [37] Roy Fox, Ari Pakman, and Naftali Tishby. Taming the noise in reinforcement learning via soft updates. In Proceedings of the Thirty-Second Conference on Uncertainty in Artificial Intelligence, UAI’16, p. 202–211, Arlington, Virginia, USA, 2016. AUAI Press.
- [38] Evelyn F. Keller and Lee A. Segel. Model for chemotaxis. Journal of Theoretical Biology, Vol. 30, No. 2, pp. 225–234, 1971.
- [39] Kevin J. Painter. Mathematical models for chemotaxis and their applications in self-organisation phenomena. Journal of Theoretical Biology, Vol. 481, pp. 162–182, 2019. Celebrating the 60th Birthday of Professor Philip Maini.
- [40] Andrew D Renault, Prabhat S Kunwar, and Ruth Lehmann. Lipid phosphate phosphatase activity regulates dispersal and bilateral sorting of embryonic germ cells in drosophila. Development, Vol. 137, No. 11, pp. 1815–1823, 2010.
- [41] Trung V. Phan, Ryan Morris, Matthew E. Black, Tuan K. Do, Ke-Chih Lin, Krisztina Nagy, James C. Sturm, Julia Bos, and Robert H. Austin. Bacterial route finding and collective escape in mazes and fractals. Physical Review X, Vol. 10, p. 031017, Jul 2020.

- [42] Martin L. Puterman. Markov Decision Processes: Discrete Stochastic Dynamic Programming. John Wiley & Sons, Inc., USA, 1st edition, 1994.
- [43] Timothy EJ Behrens, Timothy H Muller, James CR Whittington, Shirley Mark, Alon B Baram, Kimberly L Stachenfeld, and Zeb Kurth-Nelson. What is a cognitive map? organizing knowledge for flexible behavior. Neuron, Vol. 100, No. 2, pp. 490–509, 2018.
- [44] Melanie E Moses, Judy L Cannon, Deborah M Gordon, and Stephanie Forrest. Distributed adaptive search in t cells: lessons from ants. Frontiers in immunology, Vol. 10, p. 1357, 2019.
- [45] David H Wolpert and William G. Macready. No free lunch theorems for search. Technical Report 12, 1995.
- [46] Kevin Lang and Geoffrey E Hinton. Dimensionality reduction and prior knowledge in e-set recognition. In D. Touretzky, editor, Advances in Neural Information Processing Systems, Vol. 2. Morgan-Kaufmann, 1989.
- [47] Xiaojin Zhu, Zoubin Ghahramani, and John D Lafferty. Semi-supervised learning using gaussian fields and harmonic functions. In Proceedings of the 20th International conference on Machine learning (ICML-03), pp. 912–919, 2003.
- [48] Hitoshi Iima, Yasuaki Kuroe, and Shoko Matsuda. Swarm reinforcement learning method based on ant colony optimization. In 2010 IEEE International Conference on Systems, Man and Cybernetics, pp. 1726–1733, 2010.
- [49] Joachim Weickert. A review of nonlinear diffusion filtering. In International conference on scale-space theories in computer vision, pp. 1–28. Springer, 1997.
- [50] Z Schuss, K Basnayake, and D Holcman. Redundancy principle and the role of extreme statistics in molecular and cellular biology. Physics of life reviews, Vol. 28, pp. 52–79, 2019.
- [51] Richard Dawkins. The extended phenotype: The long reach of the gene. Oxford University Press, 2016.
- [52] Alex Hopke, Allison Scherer, Samantha Kreuzburg, Michael S Abers, Christa S Zerbe, Mary C Dinauer, Michael K Mansour, and Daniel Irimia. Neutrophil swarming delays the growth of clusters of pathogenic fungi. Nature Communications, Vol. 11, No. 1, p. 2031, 2020.
- [53] Bernard J. Crespi. The evolution of social behavior in microorganisms. Trends in Ecology & Evolution, Vol. 16, No. 4, pp. 178–183, 2001.
- [54] Brian Stramer and Roberto Mayor. Mechanisms and in vivo functions of contact inhibition of locomotion. Nature Reviews Molecular Cell Biology, Vol. 18, No. 1, pp. 43–55, 2017.

- [55] Mathieu Laurière, Sarah Perrin, Matthieu Geist, and Olivier Pietquin. Learning mean field games: A survey. arXiv preprint arXiv:2205.12944, May 2022.
- [56] Catherine E Hughes and Robert JB Nibbs. A guide to chemokines and their receptors. The FEBS journal, Vol. 285, No. 16, pp. 2944–2971, 2018.
- [57] Eric Theveneau, Benjamin Steventon, Elena Scarpa, Simon Garcia, Xavier Trepât, Andrea Streit, and Roberto Mayor. Chase-and-run between adjacent cell populations promotes directional collective migration. Nature Cell Biology, Vol. 15, No. 7, pp. 763–772, Jul 1, 2013.
- [58] Sriram Ganapathi Subramanian, Pascal Poupart, Matthew E Taylor, and Nidhi Hegde. Multi type mean field reinforcement learning. arXiv preprint arXiv:2002.02513, 2020.
- [59] Saori C. Tanaka, Kenji Doya, Go Okada, Kazutaka Ueda, Yasumasa Okamoto, and Shigeto Yamawaki. Prediction of immediate and future rewards differentially recruits cortico-basal ganglia loops. Nature Neuroscience, Vol. 7, pp. 887–893, 2004.
- [60] James EM Bennett, Andrew Philippides, and Thomas Nowotny. Learning with reinforcement prediction errors in a model of the drosophila mushroom body. Nature communications, Vol. 12, No. 1, p. 2569, 2021.
- [61] Wolfram Schultz. Dopamine reward prediction-error signalling: a two-component response. Nature reviews neuroscience, Vol. 17, No. 3, pp. 183–195, 2016.
- [62] Takuya Kato and Tetsuya J. Kobayashi. Understanding adaptive immune system as reinforcement learning. Physical Review Research, Vol. 3, p. 013222, Mar 2021.
- [63] Brian D Ziebart. Modeling purposeful adaptive behavior with the principle of maximum causal entropy, 2010.
- [64] Tuomas Haarnoja, Haoran Tang, Pieter Abbeel, and Sergey Levine. Reinforcement learning with deep energy-based policies. In Proceedings of the 34th International Conference on Machine Learning - Volume 70, ICML’17, p. 1352–1361. JMLR.org, 2017.
- [65] Mohammad Gheshlaghi Azar, Vicenç Gómez, and Hilbert J. Kappen. Dynamic policy programming. Journal of Machine Learning Research, Vol. 13, No. 103, pp. 3207–3245, 2012.
- [66] Harold J. Kushner and Paul Dupuis. Numerical methods for stochastic control problems in continuous time, Vol. 24. Springer, New York, second edition edition, 2001.
- [67] Bernt Oksendal. Stochastic Differential Equations (3rd Ed.): An Introduction with Applications. Springer-Verlag, Berlin, Heidelberg, 1992.
- [68] R. Grima and T. J. Newman. Accurate discretization of advection-diffusion equations. Physical

Review E, Vol. 70, p. 036703, Sep 2004.

- [69] Hugues Meyer and Heiko Rieger. Alignment interaction and band formation in assemblies of autochemorepulsive walkers. Physical Review E, Vol. 108, p. 034604, Sep 2023.

## Supplement A: A brief review of reinforcement learning

In this section, we review entropy-regularized Markov decision process (ERMDP) and entropy-regularized reinforcement learning (ERRL) used in the main text.

### 1. Conventional MDP and RL

This subsection reviews the infinite horizon discount Markov decision process (MDP) and conventional reinforcement learning (RL) based on [34, 42], which is the foundation of ERMDP and ERL.

Conventional MDP is represented as an interaction process between an environment and an agent. Initially, at time  $t = 0$ , the environment samples an initial state  $s_0$  from an initial distribution  $p_0$ . At time  $t = 0, 1, \dots$ , the agent observes the state  $s_t$  from the environment and stochastically decides the action  $a_t$  based on the behavior policy  $\pi(\cdot|s_t)$  conditioned only on the current state  $s_t$ . The environment then samples the next state  $s_{t+1}$  according to the state transition probability  $P(\cdot|s_t, a_t)$  conditioned on the state  $s_t$  and the agent's action  $a_t$ , and returns a reward  $r_t$  based on  $s_t, a_t, s_{t+1}$  to evaluate how good the current state and action are. Although the main text formulates state transition probability  $P$  directly controlled by the agent instead of considering explicit actions, deterministic  $P$  with explicit actions  $a_t$  recovers the conventional MDP framework. MDP is mathematically defined as a tuple  $(\mathcal{S}, \mathcal{A}, P, r)$  comprising the set of possible states  $\mathcal{S}$  in the environment, the set of all possible actions  $\mathcal{A}$  by the agent, transition probability  $P : \mathcal{S} \times \mathcal{A} \rightarrow \Delta(\mathcal{S})$ , and reward function  $r : \mathcal{S} \times \mathcal{A} \rightarrow \mathbb{R}$ . For simplicity, we consider  $\mathcal{S}$  and  $\mathcal{A}$  are finite and  $r$  is bounded.

The main objective in a Markov Decision Process is to find a policy  $\pi^\dagger$  that maximizes the cumulative sum of rewards. For conventional MDP and RL, the objective is defined as expected cumulative discount reward  $\mathcal{J}[\pi]$  with discount factor  $\gamma \in [0, 1)$ :

$$\mathcal{J}[\pi] := E_{P[s_{1:\infty}, a_{0:\infty}|s_0]p_0(s_0)} \left[ \sum_{k=0}^{\infty} \gamma^k r(s_k, a_k) \right], \quad (\text{S1})$$

where the expectation is defined via the probability measure  $P[s_{1:\tau+1}, a_{0:\tau}|s_0]$  over trajectories  $(s_k, a_k)_{k=0, \dots, \tau}$  under  $\pi$  and  $P$  and an initial state probability  $p_0$ :

$$P[s_{1:\tau+1}, a_{0:\tau}|s_0] := \prod_{k=0}^{\tau} P(s_{k+1}|s_k, a_k)\pi(a_k|s_k)$$

Note we use this notation for expectation to clarify the dependence on  $\pi$  and  $P$  in the rest of this section. The objective (S1) evaluates future rewards as smaller by  $\gamma$ , which can easily account for continuous tasks observed in RL problems. It is reasonable for biological organisms with limited memory to evaluate the near future, and mammals have been believed to implement the criterion (S1) by using neurotransmitter concentrations as discount factor [59].

A representative method to find the optimal policy  $\pi^\dagger := \operatorname{argmax}_\pi \mathcal{J}[\pi]$  is the value-based approach, where indirectly determines  $\pi^\dagger$  via state value functions or action value functions. The state value function  $V^\pi : \mathcal{S} \rightarrow \mathbb{R}$  and action value function  $Q^\pi : \mathcal{S} \times \mathcal{A} \rightarrow \mathbb{R}$  for a policy  $\pi$  is defined as follows:

$$V^\pi(s) := E_{P[s_1:\infty, a_0:\infty | s_0=s]} \left[ \sum_{k=0}^{\infty} \gamma^k r(s_k, a_k) \right], \quad s \in \mathcal{S} \quad (\text{S2a})$$

$$Q^\pi(s, a) := E_{P[s_2:\infty, a_1:\infty | s_1] P(s_1 | s_0=s, a_0=a)} \left[ \sum_{k=0}^{\infty} \gamma^k r(s_k, a_k) \right], \quad s \in \mathcal{S}, a \in \mathcal{A}. \quad (\text{S2b})$$

Defining the optimal state value function  $V^\dagger : \mathcal{S} \rightarrow \mathbb{R}$  and action value function  $Q^\dagger : \mathcal{S} \times \mathcal{A} \rightarrow \mathbb{R}$  as follows:

$$V^\dagger(s) := \max_{\pi} V^\pi(s) \quad s \in \mathcal{S}, \quad (\text{S3a})$$

$$Q^\dagger(s, a) := \max_{\pi} Q^\pi(s, a) \quad s \in \mathcal{S} \quad a \in \mathcal{A}, \quad (\text{S3b})$$

$\pi^\dagger$  is explicitly written with  $Q^*$ :

$$\pi^\dagger(a|s) = \begin{cases} 1 & a = \operatorname{argmax}_{a' \in \mathcal{A}} Q^\dagger(s, a'), \\ 0 & \text{otherwise} \end{cases} \quad s \in \mathcal{S}. \quad (\text{S4})$$

Thus, maximizing  $\mathcal{J}[\pi]$  is replaced by maximizing  $V^\pi$  and  $Q^\pi$ .

One conventional method for finding  $\pi^\dagger$  is policy iteration, where with the known  $r$  and  $P$ ,  $V^\pi$  and  $Q^\pi$  can be determined via the fact that  $V^\pi$  and  $Q^\pi$  are the unique solutions to the following Bellman equations:

$$V^\pi(s) = E_{\pi(a|s)} [r(s, a) + E_{P(s'|s, a)} [\gamma V^\pi(s')]], \quad (\text{S5a})$$

$$Q^\pi(s, a) = r(s, a) + E_{P(s'|s, a)} [\gamma Q^\pi(s', a')]. \quad (\text{S5b})$$

Sometimes, the Bellman operators  $\mathcal{B}^\pi : \mathbb{R}^{|\mathcal{S}|} \rightarrow \mathbb{R}^{|\mathcal{S}|}$  and  $\mathcal{B}^\pi : \mathbb{R}^{|\mathcal{S}| \times |\mathcal{A}|} \rightarrow \mathbb{R}^{|\mathcal{S}| \times |\mathcal{A}|}$  are defined such that Eq. (S5a) and Eq. (S5b) become  $V^\pi(s) = \mathcal{B}^\pi[V^\pi](s)$  and  $Q^\pi(s, a) = \mathcal{B}^\pi[Q^\pi](s, a)$ ,

respectively. We can obtain  $V^\pi$  ( $Q^\pi$ ) by value iteration, a fixed-point iteration of  $\mathcal{B}^\pi$  (e.g.,  $V^{(n+1)} = \mathcal{B}^\pi[V^{(n)}]$ ,  $n = 1, 2, \dots$ ).

In real-world systems, including biological systems, the agent may have a limited access to reward  $r$  and state transition  $P$  in the environment. Reinforcement learning extends to the situation where agents can partially access  $r$  and  $P$  only through interactions with the environment, and learn  $\pi^\dagger$  from time series of states, actions, and rewards  $(s_t, a_t, r_t)_{t=0,1,\dots}$ . One popular method in reinforcement learning is Q-learning, a variant of TD-learning, which uses the fact that  $V^\dagger$  and  $Q^\dagger$  are the unique solutions to the following Bellman optimality equation:

$$V^\dagger(s) = E_{\pi(a|s)} \left[ r(s, a) + \gamma \max_a E_{P(s'|s,a)} [V^\dagger(s')] \right], \quad (\text{S6a})$$

$$Q^\dagger(s, a) = r(s, a) + \gamma E_{P(s'|s,a)} \max_{a'} [Q^\dagger(s', a')]. \quad (\text{S6b})$$

Q-learning approximates the expectation w.r.t.  $P$  on RHS of Eq. (S6b) using current samples and relax it with a learning rate  $\alpha_t \in [0, 1)$ :

$$Q_{t+1}(s_t, a_t) = (1 - \alpha_t)Q_t(s_t, a_t) + \alpha_t \left( r_t + \gamma \max_{a' \in \mathcal{A}} Q_t(s_{t+1}, a') \right), \quad (\text{S7a})$$

$$Q_{t+1}(s, a) = Q_t(s, a), \quad \forall (s, a) \neq (s_t, a_t). \quad (\text{S7b})$$

$(s_t, a_t, r_t)_{t=0,1,\dots}$  is generated by sampling  $a_t \sim \pi_b(\cdot|s_t)$ ,  $r_t = r(s_t, a_t)$  and  $s_{t+1} \sim P(\cdot|s_t, a_t)$ . The policy  $\pi_b$  followed by action is referred as the behavior policy, which in general differ from the target policy  $\pi^\dagger$ . Thus Q-learning is categorized into off-policy algorithms. The update  $r_t + \gamma \max_a Q_t(s_{t+1}, a) - Q_t(s_t, a_t)$  in Eq. (S7) is referred to as temporal difference (TD) error, which is thought to be represented in neural activity to achieve reinforcement learning in insects [60] and primates [61].

## 2. Entropy-regularized MDP and RL

There are two major issues with the formulation of reinforcement learning based on conventional MDPs. The first issue is that the stochastic noise generated by approximating the expected value with samples is amplified by max operator, leading to overestimation and unstable learning. The second issue is that the deterministic target policy  $\pi^\dagger$  lacks theoretical connections with exploratory behavior policies  $\pi_b$ , such as  $\varepsilon$ -greedy or Boltzmann policies, thus require additional parameter tuning. These two issues are also problematic

when applying reinforcement learning to biological systems because biological agents do not always choose deterministically action even after learned. One potential reason for this stochasticity is that biological systems are inherently stochastic, thus deterministic behavior incurs a large control cost [62].

The entropy-regularized MDP (ERMDP) addresses these issues by optimizing policies considering both rewards and control costs through policy regularization [63, 64]. One formulation of ERMDP defines the following objective  $\mathcal{J}[\pi]$  for policy  $\pi$  [37]:

$$\mathcal{J}[\pi] := E_{P[s_{1:\infty}, a_{0:\infty}|s_0]p_0(s_0)} \left[ \sum_{k=0}^{\infty} \gamma^k R^\pi(s_k, a_k) \right] \quad (\text{S8a})$$

$$R^\pi(s_k, a_k) = r(s_k, a_k) - \frac{1}{\beta} \log \frac{\pi(a_k|s_k)}{\pi_{\text{ref}}(a_k|s_k)}, \quad (\text{S8b})$$

where control penalty for  $p$  is included as KL divergence to an intrinsic policy  $\pi_{\text{ref}}$ .  $\beta \in (0, \infty)$  is the inverse control weight and smaller  $\beta$  assigns higher control cost.

The above argument holds in the case where agent directly control  $P$  [33, 65], as adapted in the main text. When the agent controls  $P$  itself, at each time  $t = 0, 1, \dots$ , the agent observes the state  $s_t \in \mathcal{S}$  from the environment and the environment then samples the next state  $s_{t+1}$  using the agents' policy  $\pi_t : \mathcal{S} \rightarrow \Delta(\mathcal{S})$  and returns  $s_{t+1}$  and a reward  $r_t$  to the agent. The objective  $\mathcal{J}$  is defined as follows:

$$\mathcal{J}[\pi] := E_{P^\pi[s_{1:\infty}|s_0]p_0(s_0)} \left[ \sum_{t=0}^{\infty} \gamma^t R^\pi(s_t, s_{t+1}) \right],$$

$$R^\pi(s_t, s_{t+1}) := r(s_t) - \frac{1}{\beta} \log \frac{\pi(s_{t+1}|s_t)}{p(s_{t+1}|s_t)}$$

$$P^\pi[s_{1:\infty}|s_0] := \prod_{t=0}^{\infty} \pi(s_{t+1}|s_t)p(s_0),$$

where for given intrinsic policy  $p : \mathcal{S} \rightarrow \Delta(\mathcal{S})$ ,  $\mathcal{J}[\pi]$  is defined only for policies  $\pi$  where  $\pi(s'|s) = 0$  for all  $s, s' \in \mathcal{S}$  where  $p(s'|s) = 0$ . The penalty for the transition from time  $t$  to  $t + 1$  is weighted by  $\gamma^t$ , the same as the reward  $r(s_t)$  at time  $t$  but it can also be weighted by  $\gamma^{t+1}$ , the same as the reward  $r(s_{t+1})$  at time  $t + 1$ , which corresponds to a parameter transformation.

Similarly to MDP, the state value function  $V^\pi : \mathcal{S} \rightarrow \mathbb{R}$  for  $\pi$  (Eq. (3)) and the optimal

state value function  $V^* : \mathcal{S} \rightarrow \mathbb{R}$  (Eq. (4)) are defined:

$$V^\pi(s) := E_{P^\pi[s_{0:\infty}|s_0=s]} \left[ \sum_{t=0}^{\infty} \gamma^t R^\pi(s_t, s_{t+1}) \middle| s_0 = s \right] \quad s \in \mathcal{S},$$

$$V^*(s) := \max_{\pi} V^\pi(s) \quad s \in \mathcal{S}.$$

Similarly, the optimal policy  $\pi^*$  maximizing  $\mathcal{J}[\pi]$  can be explicitly written using  $V^*$  (Eq. (5)):

$$\pi^*(s'|s) = \frac{p(s'|s) \exp(\beta\gamma V^*(s'))}{\sum_{s' \in \mathcal{S}} p(s'|s) \exp(\beta\gamma V^*(s'))} \quad s, s' \in \mathcal{S}.$$

The problematic max operator in the optimal policy  $\pi^\dagger$  of conventional MDP is replaced by a softmax operator, resulting in an optimal policy  $\pi^*$  that is stochastic and exploratory. The exploration level of  $\pi^*$  is determined by inverse control weight  $\beta$  and discount factor  $\gamma$ .

Similarly,  $V^\pi$  is the unique solution to the Bellman equation (S9):

$$V^\pi(s) = r(s) + E_{\pi(s'|s)} \left[ \gamma V^\pi(s) - \frac{1}{\beta} \log \frac{\pi(s'|s)}{p(s'|s)} \right] \quad s \in \mathcal{S}. \quad (\text{S9})$$

Bellman operator  $\mathcal{B}^\pi : \mathbb{R}^{|\mathcal{S}|} \rightarrow \mathbb{R}^{|\mathcal{S}|}$  is defined such that Eq. (S9) becomes  $V^\pi(s) = \mathcal{B}^\pi[V^\pi](s)$ .

We can obtain  $V^\pi$  by value iteration, a fix-point iteration of  $\mathcal{B}^\pi$ .

Based on ERMDP, we can consider reinforcement learning problem, called ERRL, where the agent only partially access to  $r$  through interaction with the environment.

Similarly,  $V^*$  is the unique solution to the Bellman optimality equation:

$$V^*(s) = r(s) + \max_{\pi} E_{\pi(s'|s)} \left[ \gamma V^*(s') - \frac{1}{\beta} \log \frac{\pi(s'|s)}{p(s'|s)} \right] \quad s \in \mathcal{S} \quad (\text{S10a})$$

$$= r(s) + \frac{1}{\beta} \log \mathcal{G}[V^*](s), \quad (\text{S10b})$$

$$\mathcal{G}[V](s) := \sum_{s' \in \mathcal{S}} p(s'|s) \exp(\beta\gamma V(s')) \quad s \in \mathcal{S}. \quad (\text{S10c})$$

Note Eq. (S10b) is without max operator.

Similarly to Q-learning (S7), we can consider a variant of TD-learning, called G-learning [37], using Eq. (S10):

$$V_{t+1}(s_t) = (1 - \alpha_t) V_t(s_t) + \alpha_t \left( r_t + \log \sum_{s' \in \mathcal{S}} p(s'|s_t) \exp(\beta\gamma V_t(s')) \right) \quad (\text{S11a})$$

$$V_{t+1}(s) = V_t(s), \quad \forall s \neq s_t, \quad (\text{S11b})$$

where  $\alpha_t \in (0, 1)$  is a learning rate and  $(s_t, r_t)_{t=0,1,\dots}$  is sampled as  $s_{t+1} \sim \pi_b(\cdot|s_t)$ ,  $r_t = r(s_t)$ .

In ERRL, we can use the following greedy policy  $\pi_t$  as  $\pi_b$ :

$$\pi_t(s'|s) := \frac{p(s'|s) \exp(\gamma V_t(s'))}{\sum_{s' \in \mathcal{S}} p(s'|s) \exp(\beta \gamma V_t(s'))}. \quad (\text{S12})$$

This policy corresponds to the softmax (Boltzmann) policy with preference  $\beta \gamma V_t$ . This policy is greedy: if  $V_t(s) = V^*(s)$  for all  $s$ ,  $\pi_t = \pi^*$ . Furthermore, it balances exploration and exploitation: it can choose various states early in learning while it choose states with higher  $V_t$ . Thus, in ERRL, there exists a behavior policy (S12) that is exploratory while being theoretically connected to the optimal policy, eliminating the need to adjust parameters during learning. We refer to the learning algorithm consisting of the behavior policy (S12) and value update (S11) as Greedy G-learning.

The above argument holds for other definitions of the estimated value within proportionality factor, as in the main text:  $V^*(s) \approx Z_t(s)/\beta$ .

The Bellman optimality equation (S10) is the core in Greedy G-learning (S12), (S11). Employing the continuous bijection  $Z^*(s) = \exp(\beta V^*(s))$ , we obtain a variant of Bellman optimality equation (S13a) and corresponding optimal policy (S13c):

$$Z^*(s) = \exp(\beta r(s)) \mathcal{G}[Z^*](s), \quad (\text{S13a})$$

$$\mathcal{G}[Z](s) := \sum_{s' \in \mathcal{S}} p(s'|s) (Z(s'))^\gamma. \quad (\text{S13b})$$

$$\pi^*(s'|s) = \frac{p(s'|s) (Z^*(s'))^\gamma}{\mathcal{G}(s)}, \quad (\text{S13c})$$

We see inverse control weight  $\beta$  is the scaling factor for reward  $r$  [64] in Eq. (S13a), indicating that lower control cost is equivalent to estimating the rewards as higher.

Similarly to Greedy G-learning, based on Eqs. (S13a), (S13c), we obtain a variant of TD-learning (S14) with greedy behavior policy (S15), called Greedy Z-learning:

$$Z_{t+1}(s_t) = (1 - \alpha_t) Z_t(s_t) + \alpha_t \exp(\beta r(s_t)) \sum_{s' \in \mathcal{S}} p(s'|s_t) Z_t^\gamma(s'), \quad (\text{S14a})$$

$$Z_{t+1}(s) = Z_t(s), \quad \forall s \neq s_t, \quad (\text{S14b})$$

where  $\alpha_t \in (0, 1)$  is a learning rate and  $(s_t, r_t)_{t=0,1,\dots}$  are sampled by  $s_{t+1} \sim \pi_t(\cdot|s_t)$ ,  $r_t = r(s_t)$ , and

$$\pi_t(s'|s) := \frac{p(s'|s) Z_t^\gamma(s')}{\sum_{s' \in \mathcal{S}} p(s'|s) Z_t^\gamma(s')}. \quad (\text{S15})$$

## Supplement B: Derivation of the update equations and continuous limits

### 1. Derivation of the intrinsic cue concentraion updates

Eq. (8) (Eq. (10)) is derived as a semi-gradient descent on the cost  $\mathcal{C}[Z_t]$  (7) ((11), resp):

$$Z_{t+1}(s) - Z_t(s) = -\alpha \nabla_Z \mathcal{C}[Z_t](s) \quad (\text{S1a})$$

$$= -\alpha N \mu^{\pi_t}(s) (Z_t(s) - Z^*(s)) - D \sum_{s' \in \mathcal{S}} L_{ss'} Z_t(s') \quad (\text{S1b})$$

$$\approx -\alpha N \sum_{i=1}^N \frac{1}{N} \mathbb{1}_{s_t^i=s} (Z_t(s) - Z^*(s)) - D \sum_{s' \in \mathcal{S}} L_{ss'} Z_t(s') \quad (\text{S1c})$$

$$\begin{aligned} &\approx -\alpha \sum_{i=1}^N \mathbb{1}_{s_t^i=s} \left( Z_t(s) - \exp(\beta r(s)) \sum_{s' \in \mathcal{S}} p(s'|s) Z_t^\gamma(s') \right) \\ &\quad - D \sum_{s' \in \mathcal{S}} L_{ss'} Z_t(s'). \end{aligned} \quad (\text{S1d})$$

$$\begin{aligned} &= -\alpha \sum_{i=1}^N \mathbb{1}_{s_t^i=s} (Z_t(s) - \rho_t(s_{t+1}^i|s) \exp(\beta r(s)) Z_t^\gamma(s_{t+1}^i)) \\ &\quad - D \sum_{s' \in \mathcal{S}} L_{ss'} Z_t(s'), \end{aligned} \quad (\text{S1e})$$

where,  $\rho_t(s'|s) := p(s'|s)/\pi_t(s'|s)$  ( $s, s' \in \mathcal{S}$ ) is the importance sampling ratio [35] that corrects the deviation between the behavior policy  $\pi_t$  and the target policy  $p$ . In Eq. (S1c), the stochastic gradient descent is applied by approximating the expectation with respect to the stationary distribution  $\mu^{\pi_t}$  using samples  $(s_t^i)_{i=1}^N$  following a Markov process with policy  $\pi_t$ . In Eq. (S1d), the unknown optimal value  $Z^*$  is replaced by the reward  $(r(s_t^i))_{i=1}^N$  and the current estimate  $Z_t$  by using the fact that  $Z^*$  is the unique solution of the Bellman optimality equation (S13a) ((S10b), resp). In Eq. (S1e), the policy (6) ((9), resp) is used. Eqs. (S1e) and (S1d) is mathematically equivalent, but in this paper, we use Eq. (S1d) to simplify the calculation of the continuous limit in Appendix. (B 2).

### 2. Derivation of the continuous limits

In this section, for simplicity, we derive the continuous limits (12), (13) and (14) by restricting to the one-dimensional Euclidean space. When considering the continuous limits of the coupled Eqs. (6), (8) (Eqs. (9), (10)),

As a discrete approximation of the one-dimensional Euclidean space, we consider a one-dimensional lattice  $S^h := \{0, \pm h, \pm 2h, \dots\}$  with a uniform spacing  $h \in \mathbb{R}_{>0}$ , and define a distributed learning by an agent population on the state space  $\mathcal{S} = S^h$ . We define the intrinsic transition probability  $p$  on  $S^h$  as a lazy random walk, similar to Sec. (IV):

$$p^h(x|x) = \varepsilon^h(x) = O(h), \quad (\text{S2a})$$

$$p^h(x \pm h|x) = \frac{1 - \varepsilon^h(x)}{2}, \quad (\text{S2b})$$

where we assume that  $\varepsilon^h(x) \rightarrow 0$  as  $h \rightarrow 0$ , indicating that the smaller the spacing  $h$ , the less likely it is to stay at the same vertex.

*a. Continuous limit of agents' motility*

Given the intrinsic cue concentration  $Z(t', \cdot) : \mathbb{R} \rightarrow \mathbb{R}_{\geq 0}$ , we consider agents with  $p$  (S2) and policy (9) dependent on  $Z$  on  $S^h$ . The trajectory of an agent's position is a Markov chain  $(\xi_n^h)_{n=0,1,\dots}$  on  $S^h$  with the following transition probability  $\pi^h(\cdot|\cdot)$ :

$$\pi^h(x|x) = \varepsilon^h(x) \exp(\gamma Z(t', x)) / \mathcal{Z}^h(x), \quad (\text{S3a})$$

$$\pi^h(x \pm h|x) = \frac{1 - \varepsilon^h(x)}{2} \exp(\gamma Z(t', x \pm h)) / \mathcal{Z}^h(x), \quad (\text{S3b})$$

$$\mathcal{Z}^h(x) = \varepsilon^h(x) \exp(\gamma Z(t', x)) + \frac{1 - \varepsilon^h(x)}{2} (\exp(\gamma Z(t', x + h)) + \exp(\gamma Z(t', x - h))), \quad (\text{S3c})$$

where  $Z(t', \cdot)$  is assumed to be constant over times  $n = 0, 1, \dots$

We define the time step  $\Delta t^h := h^2 / \sigma^2$  depending on spacing  $h$ , for  $n = 0, 1, \dots$ , the position increment  $\Delta \xi_n^h := \xi_n^h - \xi_{n-1}^h$  satisfies local consistency [66]:

$$E[\Delta \xi_n^h] = h(\pi^h(x + h|x) - \pi^h(x - h|x)) \quad (\text{S4a})$$

$$= \gamma h^2 \partial_x Z(t', x) + O(h^4) \quad (\text{S4b})$$

$$= \gamma \sigma^2 \partial_x Z(t', x) \Delta t^h + O((\Delta t^h)^2), \quad (\text{S4c})$$

and

$$E[(\Delta \xi_n^h - E[\Delta \xi_n^h])^2] = E[(\Delta \xi_n^h)^2] - (E[\Delta \xi_n^h])^2 \quad (\text{S5a})$$

$$= h^2 + O(h^4) \quad (\text{S5b})$$

$$= \sigma^2 \Delta t^h + O((\Delta t^h)^2), \quad (\text{S5c})$$

where in Eqs. (S4b), (S5b), the Taylor series w.r.t.  $h$  is used as follows:

$$\pi^h(x \pm h|x) = \frac{1 - \varepsilon^h(x)}{2} \exp(\gamma Z(t', x)) (1 \pm \gamma h \partial_x Z(t', x) + O(h^2)) (\exp(\gamma Z(t', x))(1 + O(h^2)))^{-1} \quad (\text{S6a})$$

$$= \frac{1}{2} - \frac{\varepsilon^h(x)}{2} \pm \frac{\gamma}{2} h \partial_x Z(t', x) + O(h^2), \quad (\text{S6b})$$

where in Eq. (S6a), the Taylor series w.r.t.  $h$  are performed for  $\exp(\gamma Z(t', x \pm h))$  and  $Z^h(x)$ .

As  $\Delta t^h \rightarrow 0$  ( $h \rightarrow 0$ ) and local consistency (S4c) and (S5c) is satisfied, if the Markov chain  $(\xi_n^h)_{n=0, \dots}$  satisfies the initial condition  $\xi_0^h = x$ , the solution  $\xi^h(t) := \xi_n^h$ ,  $t \in [t_n^h, t_{n+1}^h)$ ,  $t_n^h := t' + \sum_{i=0}^{n-1} \Delta t^h$  of the corresponding time-continuous Markov chain converges to the solution of the following stochastic differential equations [66, Theorem 4.1]:

$$dx(t) = \gamma \sigma^2 \partial_x V(t, x) dt + \sigma dW(t) \quad (\text{S7})$$

with  $x(t') = x$ , where  $W(t)$  is a one-dimensional standard Wiener process. This indicates that an agent following a biased random walk weighted by the exponent of the surrounding intrinsic cue concentration corresponds to an agent following a random walk climbing the gradient of the intrinsic cue concentration in the space-time continuous limit.

The Fokker-Planck-Kolmogorov forward equation for the probability density  $\rho(t, x)$  of random variable  $x$  following SDE (S7) is given [67] by

$$\partial_t \rho(t, x) = -\nabla \cdot (\gamma \sigma^2 \nabla Z(t, x) \cdot \rho(t, x)) + \frac{\sigma^2}{2} \nabla^2 \rho(t, x) \quad (\text{S8})$$

with  $\rho(t', x) = 1$ , yielding  $\phi(\nabla Z, \nabla \log Z) = \gamma \sigma^2 \nabla Z$  (Eq. (14)). This indicates that the distribution of agents following a random walk weighted by the exponent of the surrounding intrinsic cue concentration (6) corresponds to a diffusion-advection equation with the gradient of the concentration as drift in the space-time continuous limit [68, 69].

The FPK equation for policy (6) is derived similarly by setting  $Z(t, x) \rightarrow \log Z(t, x)$ :

$$\partial_t \rho(t, x) = -\nabla \cdot (\gamma \sigma^2 \nabla \log Z(t, x) \cdot \rho(t, x)) + \frac{\sigma^2}{2} \nabla^2 \rho(t, x) \quad (\text{S9})$$

with  $\rho(t', x) = 1$ , yielding  $\phi(\nabla Z, \nabla \log Z) = \gamma \sigma^2 \nabla \log Z$  (Eq. (13)). This indicates that the distribution of agents following a random walk weighted by the power of the surrounding concentration (9) corresponds to a diffusion-advection equation with the logarithmic gradient as drift in the limit.

*b. Continuous limit of the intrinsic cue concentration updates*

First, we consider the update of the intrinsic cue concentration  $Z_t^h : \mathbb{R} \rightarrow \mathbb{R}_{\geq 0}$  following Eq. (8) on  $S^h \subset \mathbb{R}$ . Here,  $Z_t^h(x) = Z_t^h(nh)$ ,  $x \in [nh, (n+1)h)$ ,  $n = 0, \pm 1, \dots$  and set appropriate boundary conditions without strict handling. Additionally, we approximate the number of agents  $\mu_t(x)$  at vertex  $x \in S^h$  at time  $t$ , which is a random variable, by a deterministic value  $\mu_t^h(x)$ , assuming an infinite number of agents.

With the time step  $\Delta t^h = h^2/\sigma^2$  and the learning rate  $\alpha^h(x) = \alpha\Delta t^h$ , for  $x \in S^h$ , the update of  $Z_t^h(x)$  following Eq. (8) is give by:

$$Z_{t+\Delta t^h}^h(x) - Z_t^h(x) = -\alpha^h(x)\mu_t^h(x) \left( Z_t^h(x) - \exp(\beta r(x)) \left( \sum_{y \in \{x, x \pm h\}} p^h(y|x) (Z_t^h(y))^\gamma \right) \right) + D (Z_t^h(x+h) - Z_t^h(x) + Z_t^h(x-h) - Z_t^h(x)) \quad (\text{S10a})$$

$$= -\alpha\Delta t^h \mu_t^h(x) (Z_t^h(x) - \exp(\beta r(x)) ((Z_t^h(x))^\gamma + O(h^2))) + D\sigma^2 \Delta t^h \frac{1}{h} \left( \frac{Z_t^h(x+h) - Z_t^h(x)}{h} - \frac{Z_t^h(x) - Z_t^h(x-h)}{h} \right) \quad (\text{S10b})$$

By taking the limit as  $h \rightarrow 0$ , the formal space-time continuous limit  $Z$  of  $Z_t^h$  satisfies the following partial differential equation with appropriate boundary condition:

$$\partial_t Z(t, x) = -\alpha\mu(t, x)Z(t, x) + \alpha\mu(t, x) \exp(\beta r(x))Z^\gamma(t, x) + D\sigma^2 \nabla^2 Z(t, x), \quad (\text{S11})$$

where,  $\mu(t, x)$  denotes the spatial limit of  $\mu_t^h(x)$ . When  $\mu(t, x) = N\rho(t, x)$  with  $\rho(t, x)$  following (S8), we obtain  $H(\mu, Z) = \alpha\mu Z$ ,  $G(\mu, Z, r) = \alpha\mu \exp(\beta r)Z^\gamma$  (Eq. (13)). This indicates that the distributed learning dynamics by agent population, based on immediate local concentrations and logarithmic mapping, corresponds to a diffusion equation with linear degradation and nonlinear production in the space-time limit.

Similarly, the update of  $Z_t^h(x)$  following Eq. (10) with Talor series w.r.t.  $h$  is given by:

$$Z_{t+\Delta t^h}^h(x) - Z_t^h(x) = -\alpha^h(x)\mu_t^h(x) \left( Z_t^h(x) - \beta r(x) - \left( \ln \sum_{y \in \{x, x \pm h\}} p^h(y|x) \exp(\gamma Z_t^h(y)) \right) \right) + D (Z_t^h(x+h) - Z_t^h(x) + Z_t^h(x-h) - Z_t^h(x)) \quad (\text{S12a})$$

$$= -\alpha^h(x)\mu_t^h(x) (Z_t^h(x) - \beta r(x) - \gamma Z_t^h(x) + O(h^2)) + D (Z_t^h(x+h) - Z_t^h(x) + Z_t^h(x-h) - Z_t^h(x)), \quad (\text{S12b})$$

and the formal space-time continuous limit  $Z$  of  $Z_t^h$  satisfies the following PDE with appropriate boundary condition:

$$\partial_t Z(t, x) = -\alpha(1 - \gamma)\mu(t, x)Z(t, x) + \alpha\beta\mu(t, x)r(x) + D\sigma^2\nabla^2 Z(t, x), \quad (\text{S13})$$

yielding  $H(\mu, Z) = \alpha(1 - \gamma)\mu Z$ ,  $G(\mu, Z, r) = \alpha\beta\mu r$  (Eq. (14)). This indicates that the distributed learning dynamics by agent population, based on immediate local concentrations and linear mapping, corresponds to a diffusion equation with linear degradation and linear production in the space-time limit.

### Supplement C: Supplemental experiments

In this section, supplemental experiments for Sec. IV are shown.

#### 1. Maze solving with other couplings

In sec. IV A we have examined the optimality in couplings of policy and update by maze-solving with the optimal log-exp coupling (6) (8), and with the non-optimal log-lin coupling (9), (8). In this subsection, we demonstrate maze solving by the other couplings used in Sec. IV B: the optimal lin-lin coupling (9), (10) and the non-optimal lin-exp coupling (9), (8).

First, Figure S1 shows snapshots of the concentration distribution  $Z_t$ , agent distribution  $\mu_t$ , and the time average regularized reward distribution  $(R^i[s_{0:t}^i, \pi_{0:t-1}])_{i=1}^N$  at  $t = 21, 1001, 15001$  for one trial with the optimal lin-lin coupling (9), (10).

A qualitatively similar behavior as the optimal log-exp coupling (6), (8) is observed. Agents eventually similarly accumulate near the goal and have similar distribution of  $R^i$  (Figure S1  $t = 15001$ ), though the concentration is more gradual than the log-exp coupling, as observed in a chain graph (Figure 5 (b)).

Next, Figure S2 shows snapshots of the concentration distribution  $Z_t$ , agent distribution  $\mu_t$ , and the time average regularized reward distribution  $(R^i[s_{0:t}^i, \pi_{0:t-1}])_{i=1}^N$  at  $t = 21, 1001, 15001$  for one trial with the non-optimal lin-exp coupling (9), (8).

The non-optimal lin-exp coupling exhibits qualitatively different behavior compared to the other three couplings, both in transient and steady states. In the transient state, the

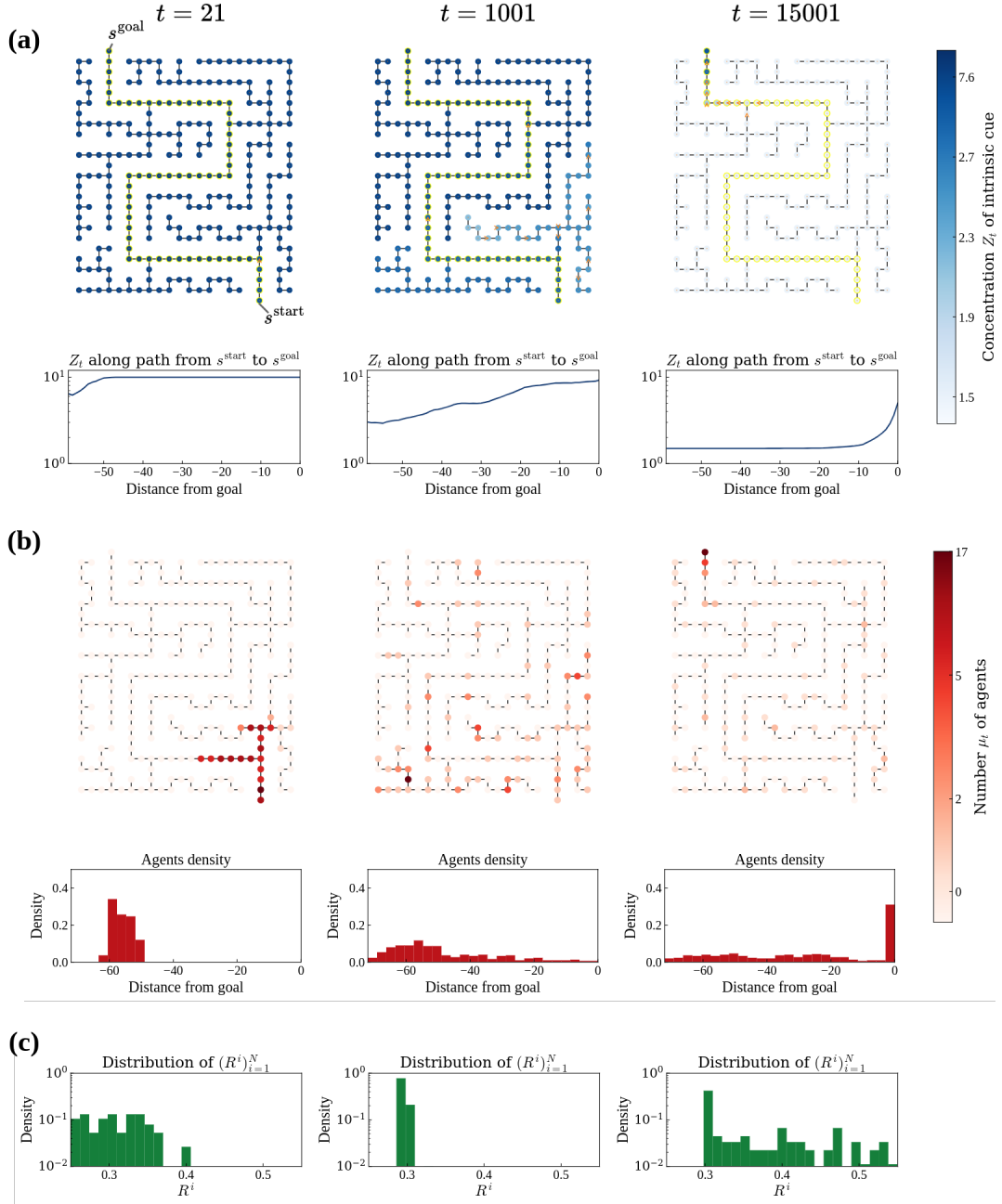


FIG. S1. Snapshots of one trial at  $t = 21, 1001, 15001$  evolved according to the optimal lin-lin coupling (9), (10). (a) Intrinsic cue concentration  $Z_t$ , (b) Agent distribution  $\mu_t$ , (c) The time average regularized reward distribution  $(R^i[s_{0:t}^i, \pi_{0:t-1}])_{i=1}^N$ . In (a) and (b), graphs are colored by the values at the vertices. Arrows in graphs of (a) indicate the gradient direction. Below graph of (a), the values are plotted along the shortest path (in yellow) against the distance from the goal. Below graphs of (b), agent distribution relative to the distance to the goal.  $\alpha = 0.0098$ ,  $N = 100$ ,  $D = 0.01$ ,  $\gamma = 0.8$ ,  $Z_0 = 10.0$ ,  $\varepsilon = 0.5$ ,  $\beta$ ,  $r(s^{\text{goal}}) = 1.5$ ,  $r(s) = 0.3$  for  $s \neq s^{\text{goal}}$ .

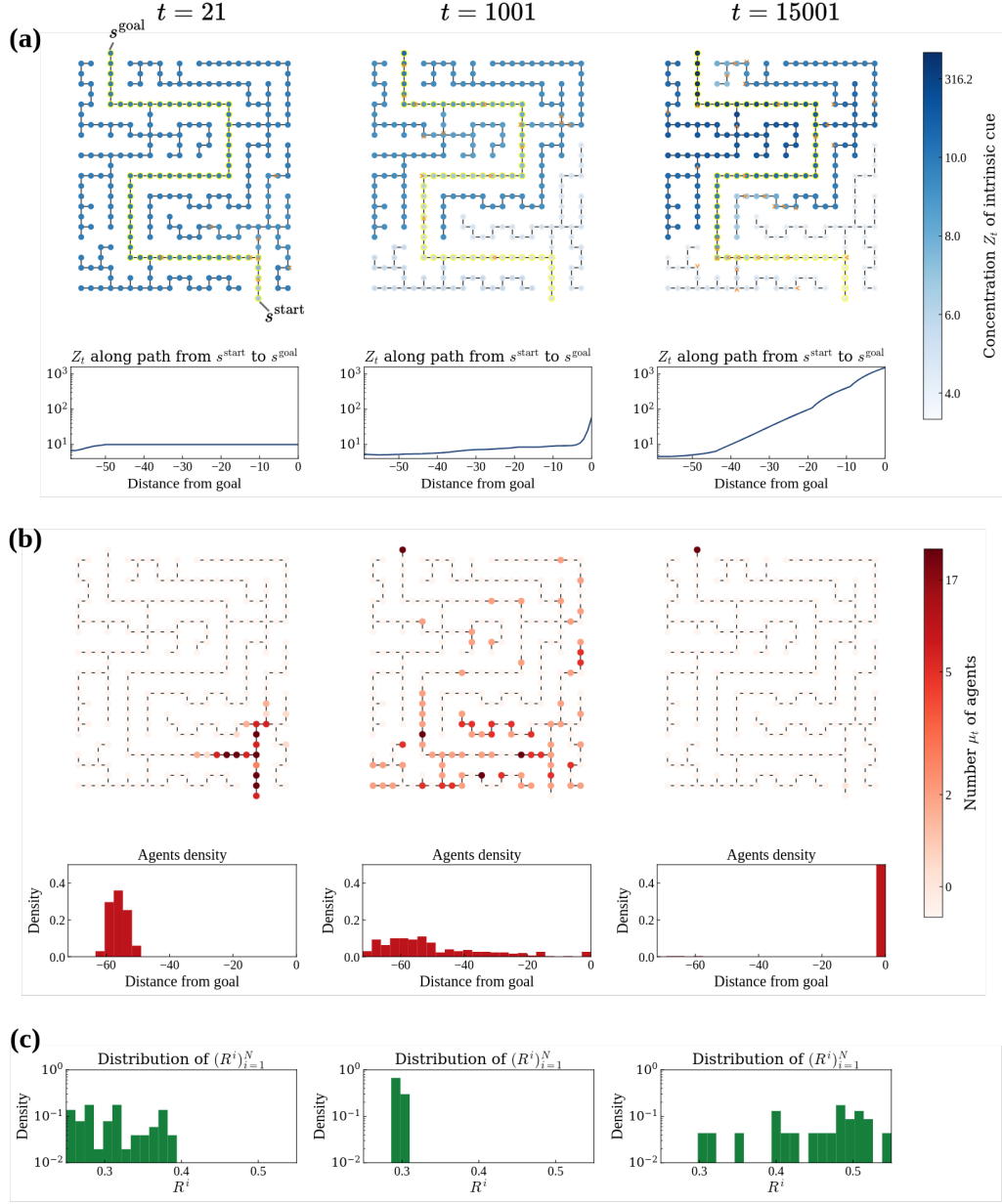


FIG. S2. Snapshots of one trial at  $t = 21, 1001, 15001$  evolved according to the non-optimal lin-exp coupling (9), (8). (a) Intrinsic cue concentration  $Z_t$ , (b) Agent distribution  $\mu_t$ , (c) The time average regularized reward distribution  $(R^i[s_{0:t}^i, \pi_{0:t-1}])_{i=1}^N$ . In (a) and (b), graphs are colored by the values at the vertices. Arrows in graphs of (a) indicate the gradient direction. Below graph of (a), the values are plotted along the shortest path (in yellow) against the distance from the goal. Below graphs of (b), agent distribution relative to the distance to the goal.  $\alpha = 0.0098$ ,  $N = 100$ ,  $D = 0.01$ ,  $\gamma = 0.8$ ,  $Z_0 = 10.0$ ,  $\varepsilon = 0.5$ ,  $\beta$ ,  $r(s^{\text{goal}}) = 1.5$ ,  $r(s) = 0.3$  for  $s \neq s^{\text{goal}}$ .

intrinsic cue production speed by agents is faster than that of the optimal log-exp coupling, despite both following an exponentially producing update (Figure S2 (a)  $t = 1001$ ). In the steady state, as observed in a chain graph (Figure 5 (b), (c)), agents generate a globally high, gradual gradient (Figure S2 (a)  $t = 15001$ ), strongly accumulate at the goal (Figure S2 (b)  $t = 15001$ ), and have as high  $R^i$  as the optimal couplings (Figure S2 (c)  $t = 15001$ ). Unlike the other couplings, the concentration does not align with the distance from the goal, implying the unexplored area in the steady state.

These result can be qualitatively understand by considering that the agents' policies become almost deterministic even in the transient state, as suggested in Sec. IV B. Even with few agents at the goal, they transition almost deterministically to the goal and continue producing intrinsic cue despite diffusion. Agents that have not yet reached the goal also transition with high probability to vertices with increased concentration due to diffusion from the goal, approaching the goal before degrading the intrinsic cue at unexplored vertices. As a result, without sufficient exploration, agents remain at the goal, showing  $R^i$  values close to those of the deterministic policy.

While the non-optimal lin-exp coupling may appear advantageous by allowing agents to accumulate at the goal faster than the optimal couplings, it is important to note the drawback of its nearly deterministic policy concerning temporal control costs. For instance, agents newly placed far from the goal incur high control costs due to the deterministic nature, but hardly receive rewards, resulting a low expected discounted cumulative reward  $V^\pi$  (c.f. Fig. S3 (a)). This illustrates the metric differences: accumulating at the goal after a long time yields a high time average reward  $R^i$ , but achieving a high discounted cumulative reward  $V^\pi$  requires quickly reaching the goal with low control costs.

## 2. Supplemental figures for Section IV B

In this section, supplementary figures for Sec. IV B are shown to confirm that the optimal couplings have larger state values  $V^\pi$  than the non-optimal couplings across all vertices, maintaining a balanced distribution of reward and penalty components.

First, Figure S3 (a) shows the state value  $V^\pi$  at vertex  $s^0$  of each policy  $\pi[\tilde{Z}_T]$  with  $\beta \in [0.25, 2.6]$  and Figure 5 (b) shows the relationship between the reward component  $V_{\text{reward}}^\pi(s^0)$  and the penalty component  $V_{\text{penalty}}^\pi(s^0)/\beta$  of  $V^\pi(s^0)$ .  $V_{\text{penalty}}^\pi(s^0)$  is almost the

same as  $V_{\text{penalty}}^\pi(s^{19})$ , but  $V_{\text{reward}}^\pi(s^0)$  is smaller than  $V_{\text{reward}}^\pi(s^{19})$  (Figure S3 (b)). This is because  $V_{\text{reward}}^\pi$  places more weight on rewards received near the initial time, which are smaller for vertices farther from the goal  $s^{19}$ . The smaller  $V_{\text{reward}}^\pi$  result in lower  $V^\pi$  for the non-optimal lin-exp coupling, especially with larger  $\beta$  (Figure S3 (a)).

Next, Figure S3 (c) shows the average state value  $V^\pi$  over  $\mathcal{S}$  of each policy  $\pi[\tilde{Z}_T]$  with  $\beta \in [0.25, 2.6]$  and Figure 5 (d) shows the relationship between the reward component  $V_{\text{reward}}^\pi$  and the penalty component  $V_{\text{penalty}}^\pi/\beta$  of the average. This result is intermediate between those of vertex  $s^{19}$  and vertex  $s^0$ .

These results confirm that the optimal couplings exhibits larger state value  $V^\pi$  across all vertices compared to the non-optimal couplings, maintaining a balance between reward and penalty components, as evident from the theoretical optimality (4).

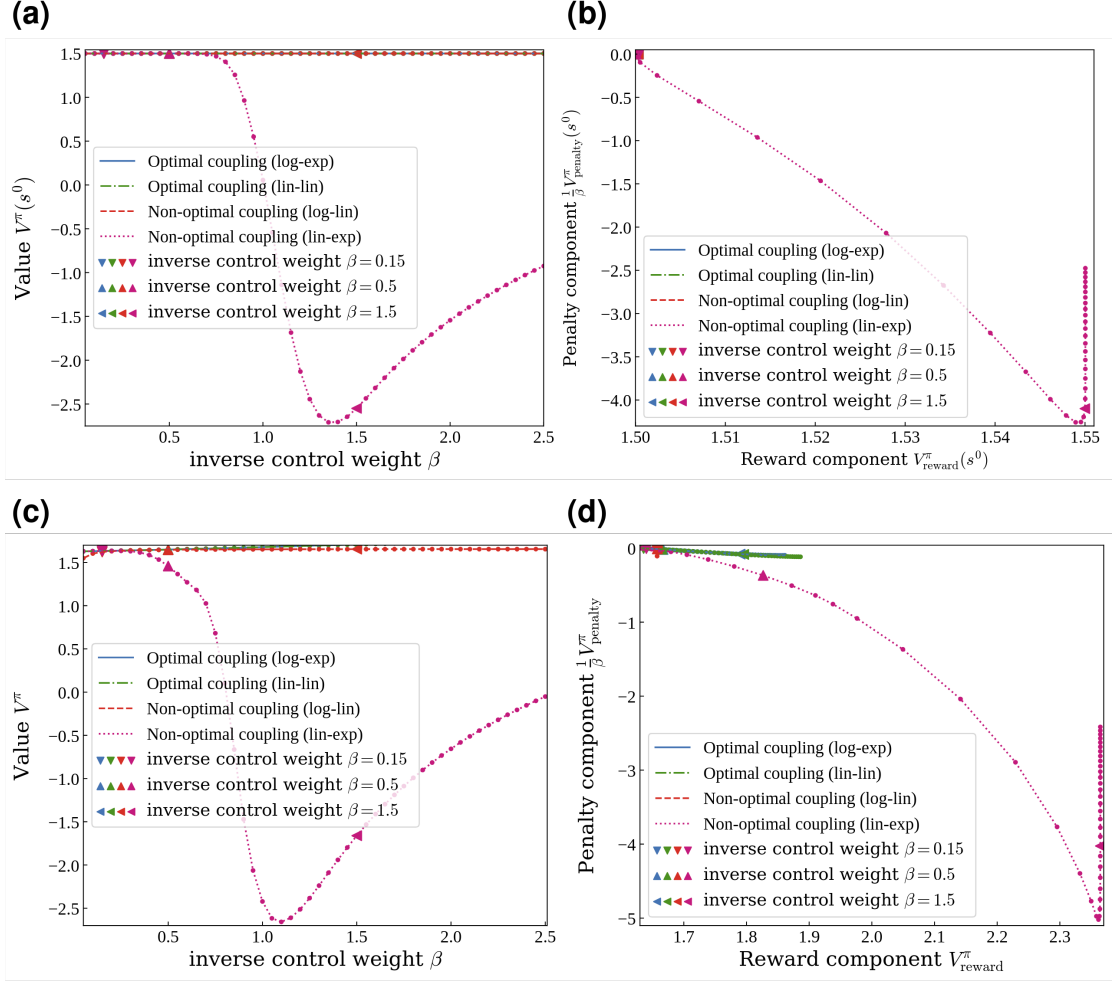


FIG. S3. (a) State value  $V^\pi(s^0)$  at vertex  $s^0$  for each policy  $\pi[\tilde{Z}_T]$  based on the trial-average steady concentration  $\tilde{Z}_T$  for the four couplings with  $\beta \in [0.25, 2.5]$ . (b) The relationship between the reward  $V_{\text{reward}}^\pi(s^0)$  and penalty component  $V_{\text{penalty}}^\pi(s^0)/\beta$  of  $V^\pi(s^0)$  for the four couplings with  $\beta \in [0.25, 2.5]$ . (c) Average of state value  $V^\pi(s^0)$  over  $\mathcal{S}$  for  $\pi[\tilde{Z}_T]$  based on  $\tilde{Z}_T$  for the four couplings with  $\beta \in [0.25, 2.5]$ . (d) The relationship between the reward  $V_{\text{reward}}^\pi$  and penalty component  $V_{\text{penalty}}^\pi/\beta$  of the average of  $V^\pi$  for the four couplings with  $\beta \in [0.25, 2.5]$ .  $N = 500$ ,  $\varepsilon = 0.5$ ,  $\alpha = 0.00196$ ,  $D = 0.01$ ,  $\gamma = 0.8$ ,  $r(s) \in \{0.3, 1.0\}$ ,  $\beta \in [0.25, 2.65]$ .